NASA CR-121249

THE EFFECT OF THERMAL CYCLING ON THE STRUCTURE AND PROPERTIES OF A Co, Cr, Ni – TaC DIRECTIONALLY SOLIDIFIED EUTECTIC COMPOSITE

BY

F. M. DUNLEVEY and J. F. WALLACE

CASE WESTERN RESERVE UNIVERSITY

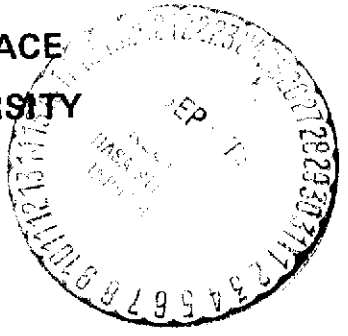

PREPARED FOR

NATIONAL AERONAUTICS AND SPACE ADMINISTRATION

NASA LEWIS RESEARCH CENTER

GRANT NGR-36-027-035

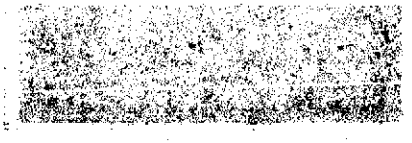

1. Report No. NASA CR-121249	2. Government Accession No.	3. Recipient's Catalog No.
4. Title and Subtitle The Effect of Thermal Cycling on the Structure and Properties of a Co,Cr,Ni-TaC Directionally Solidified Eutectic Composite		5. Report Date September 1, 1973 6. Performing Organization Code
7. Author(s) F.M. Dunlevey and J.F. Wallace		8. Performing Organization Report No. 10. Work Unit No.
9. Performing Organization Name and Address Case Western Reserve University Cleveland, Ohio 44106		11. Contract or Grant No. NGR-36-027-035
12. Sponsoring Agency Name and Address National Aeronautics and Space Administration Washington, D.C. 20546		13. Type of Report and Period Covered Contractor Report 9/71-9/73 14. Sponsoring Agency Code

15. Supplementary Notes

Project Manager, R.L. Ashbrook, Materials and Structures Division, NASA, Lewis Research Center, Cleveland, Ohio 44135

16. Abstract

A Co,Cr,Ni-TaC directionally solidified eutectic composite was subjected to thermal fatigue between 427-1093° C. The material suffered degradation in microstructure and elevated temperature mechanical properties. The loss in properties varied with the maximum cycling temperature and number of cycles. This behavior is attributed to the increasing solubility of the TaC in the matrix with temperature from 0.4% at room temperature to 2.2% at 1200° C. During the thermal cycling, the TaC is subjected to solution and reprecipitation which form serrations on the fibers since the easy growth planes of the TaC are not coincident with the fiber faces exposed to the matrix.

17. Key Words (Suggested by Author(s)) Composites Eutectics Thermal Fatigue Cobalt Alloys Tantalum Carbide	18. Distribution Statement Unclassified-unlimited		
19. Security Classif. (of this report) Unclassified	20. Security Classif. (of this page) Unclassified	21. No. of Pages 76	

NASA CR-121249

THE EFFECT OF THERMAL CYCLING ON THE STRUCTURE AND PROPERTIES OF A Co, Cr, Ni – TaC DIRECTIONALLY SOLIDIFIED EUTECTIC COMPOSITE

BY

F. M. DUNLEVEY and J. F. WALLACE
CASE WESTERN RESERVE UNIVERSITY

PREPARED FOR

NATIONAL AERONAUTICS AND SPACE ADMINISTRATION

NASA LEWIS RESEARCH CENTER
GRANT NGR-36-027-035

SUMMARY

A Co,Cr,Ni matrix, TaC reinforced, directionally solidified eutectic composite was cast in a Bridgeman type furnace as 1.25 cm rounds. These composites were subjected to thermal fatigue between 427-1093° C for up to 5000 cycles of two minute duration, and tested in stress rupture between 704 and 1204° C.

The stress rupture properties of the alloy were decreased by the thermal cycling. This loss in stress rupture properties varied with the number of cycles; the loss in properties after about 200 cycles was relatively high. The stress rupture strength improved with further cycling up to 2000 cycles and decreased for a larger number of cycles. The TaC fibers in the cycled material developed surface serrations which increased in severity with the maximum cycling temperature and the number of cycles. The formation of these serrations is attributed to the increasing solubility, from 0.4% at room temperature to 2.2% at 1200° C, of the TaC fibers in the matrix. Since the easy growth planes of the TaC fibers were not coincident with the fiber faces exposed to the matrix, the TaC which was dissolved and reprecipitated during thermal cycling formed these serrations on the easy growth planes

of the fibers. These serrations act as notches which both reduce the tensile strength of the fibers and strain harden the matrix through the introduction of a dislocation network at the jagged fiber ribs. These two opposing effects produce an initial decrease in the stress rupture properties after a few thermal cycles, followed by an improvement in properties after an intermediate number, with eventual marked loss in strength after a large number of thermal fatigue cycles.

The formation of serrations and resultant degradation in structure and properties was unaffected by interfiber spacing, rate of temperature change on cycling, and alloy chemistry. Isothermal heat treatments up to 0.88 T_m produced no change in the phase morphology, structure or composition.

TABLE OF CONTENTS

TABLE OF CONTENTS (cont.)

LIST OF TABLES

LIST OF FIGURES

LIST OF FIGURES (cont.)

I. INTRODUCTION

With much of contemporary and future transportation heavily dependent upon the gas turbine engine, the problem of increasing the performance of these engines has been receiving considerable attention. The efficiency of the gas turbine engine is governed by Carnot's laws which predict increased performance with increasing turbine inlet temperature[1*] as illustrated by Figure 1. In a commercial aircraft engine, this increase in efficiency is reflected in a reduced specific fuel consumption or in an increase in the thrust per unit weight. With advanced aircraft operating at a turbine inlet temperature of about 1050° C[1], and with aircraft engine designers committed to a turbine inlet temperature of 1350° C before 1980, a concerted effort has been made to develop new alloys capable of withstanding these temperatures in the operation of a gas turbine engine.

Historically, the first stage turbine alloys have been the pacing items in the development of gas turbine engines but the limit of these superalloys is being approached. Conventional nickel-base superalloys, which are the most widely used in aircraft turbines today, do not perform well at temperatures above 1100° C because of resolution of

*Superscripts refer to numbered References.

the strengthening phase, γ', Ni_3Al. Conventional cobalt-base superalloys, hardened by the formation of stable carbides, perform better than the nickel alloys at elevated temperatures but fall considerably short of the future goals. Refractory metal alloys generally exhibit severe oxidation problems at elevated temperatures and ceramic materials suffer from low temperature brittleness and notch sensitivity. Thus, substantial attention is being directed toward the development of composite materials for use in future first stage turbine applications[2].

The class of composite materials which show large promise are the in-situ composites, specifically, the directionally solidified eutectics (DSE). These materials generally have an aligned two phase structure consisting of a hard, brittle reinforcement phase in a matrix of a more ductile material. The aligned structure is formed on unidirectional solidification from a homogeneous liquid phase. The advantages of the DSE alloys over infiltrate or pressed powder composites are:

a) Since the composites are formed on solidification, an equilibrium process, they possess excellent thermodynamic stability at temperatures near the melting point.

b) No wetting problems exist in the fabrication of the alloys.

c) The reinforcement phase, when fibrous, are perfect

single crystals, and inherently stronger than the wires or fibers of the synthetic composites.

d) A Hall-Petch type strengthening, where the strength varies with the reciprocal square root of the dispersoid spacing, is observed in most DSE alloys.

On the other hand, some disadvantages are associated with the production of DSE alloys. The coupled growth, necessary to develop the composite structure in a eutectic alloy, can take place only at a planar liquid-solid interface. Mollard and Flemings[3] have shown that the critical condition for the stability of the planar interface is

$$\frac{G}{R} > \frac{m(C_e - C_o)}{D} ,$$

where G is the temperature gradient at the interface; R, the rate of interface advance; m, the slope of the liquidus; C_e, the amount of solute at the eutectic composition; C_o, the amount of solute in the alloy; and D, the liquid diffusion coefficient. Thus, coupled growth is stabilized under conditions of high gradient, low growth rate, and low impurity content with respect to the eutectic composition. These restrictions place the production of DSE alloy composites at a disadvantage since:

a) The DSE can be alloyed only to a limited extent.

b) The production of complex shapes, such as airfoil sections, will require special equipment to maintain

constant values of G and R.

c) Very little flexibility occurs in the volume fraction, dimensions, and geometry of the reinforcement phase.

Of the fibrous composites investigated, the cobalt- and nickel-base monocarbide (MC) systems show the most promise for future first stage turbine applications in terms of a balanced interrelation of elevated temperature mechanical properties, ductility, and oxidation resistance. Table I lists a summary of some available physical properties data on MC eutectic systems[4].

A cobalt alloy matrix, reinforced by TaC fibers offers the best mechanical properties above 1100° C of the MC systems reported[5-11], and the melting temperature of the Co-TaC system (1402° C) is the highest of the cobalt or nickel MC systems investigated. The predicted density of Co-TaC is 9.4 g/cm^3, which is only slightly higher than that of the conventional superalloys now in service. The large difference between the thermal expansion coefficients of the cobalt alloy matrix ($\approx 18 \times 10^{-6}/\ ^{o}C$) [12] and the TaC phase ($\approx 6 \times 10^{-6}/\ ^{o}C$)[13] has caused some concern for the stability of these alloys under conditions of thermal fatigue[14,15]. Breinan[12] has reported mechanical and microstructural degradation in the system Co,Cr,Ni-TaC when cycled between 400-1120° C. Bibring[16] has reported the satisfactory performance of Co,Cr,Ni-TaC and Ni,Cr-TaC

alloys, thermally cycled between 250-1070° C. Tests by Benz[17] have shown that the Co,Cr-TaC system, which is unstabilized with respect to the HCP ⟷ FCC transformation of the cobalt matrix, suffers degradation of the elevated temperature mechanical properties after cycling between 95-1093° C. On the other hand, the alloy Co50B3W (General Electric Company designation), stabilized by the addition of 9.5% nickel, actually showed an initial improvement in the stress rupture properties when cycled between 95-1093° C.

Thus, in the absence of matrix allotropy, Bibring and Benz have detected no damage from thermal fatigue, while Breinan, in similar alloys, has seen fiber fragmentation after thermal cycling. Breinan attributes the damage that he noted to the cyclic elastic stresses arising from $\Delta T \Delta \alpha$ thermal mismatch strains. It is felt that the solution to this problem can not be this simplified since the temperature difference employed by Breinan was considerably lower than that of either Bibring or Benz.

A comparison of the elevated temperature mechanical properties data of the best conventional turbine blade alloys (TRW-NASA VI-A[18] and D.S. Mar M-200[19]) and the best DSE alloys (Ni,Al,Cr-Ni_3Nb[20] and Co50B6W[17]) is shown by Figure 2. In the high temperature region, the DSE alloys show a clear superiority, but the intermediate temperature properties of the TaC reinforced Co50B6W alloy are comparatively low. Because of the importance of the DSE alloys

to the gas turbine industry, considerable research is needed to develop the full potential of these alloys. This investigation was, in particular, directed at:

a) studying the effects of thermal fatigue on TaC reinforced DSE cobalt-base alloys in terms of microstructural changes and alteration of mechanical properties;

b) developing a mechanism to explain the behavior observed in TaC reinforced DSE alloys as a result of thermal cycling; and

c) evaluating the suitability of TaC reinforced superalloy matrix DSE alloys for use in gas turbine engines up to 1200° C.

II. EXPERIMENTAL PROCEDURE

A) Initial Melting

As an initial step prior to directional solidification, the elemental materials were melted and cast into ingots that were chemically homogeneous and had a convenient shape for use in the directional solidification apparatus. The purity, supplier, and form of the raw metallic charge materials are listed in Table II. Initial melting of the 1.5 kg heats was conducted at a pressure of 0.5 atmosphere in a 50 kW, 10kHz induction furnace using calcia-stabilized zirconia crucibles. The atmosphere employed was commercially pure argon backfilled into the melting-pouring chamber after evacuation to 10 microns. The temperature was monitored optically and accurate to $\pm 25^{\circ}$ C. The cobalt and nickel and any additions in powder form were initially melted. At 1650° C the tantalum and chromium were added to the liquid. Before pouring, the melt was held at 1800° C for about five minutes to insure the complete solution of the refractory metals. The ingot molds were conventional zircon shell molds preheated to 870° C. Each ingot mold assembly yielded six sound bars 1.15 cm in diameter and 16 cm long, which were sandblasted before

directional solidification.

B) Directional Solidification

The ingots were remelted and then directionally solidified in a modified Bridgeman type furnace shown in Figure 3 and schematically in Figure 4. Listed in Table III are the materials specifications and dimensions for the directional solidification furnace. The recrystallized alumina crucible was heated by radiation from the graphite susceptor. The temperature gradient at the liquid-solid interface was determined by lowering a small sheathed thermocouple slowly into the liquid. The temperature profile in the liquid is shown in Figure 5 and the gradient at the interface was measured at 90° C/cm ±10%. Power was supplied by a 7.5 kW radio frequency generator operating at 400 kHz. At this frequency, all of the inductive coupling was in the susceptor which provided little convective mixing in the liquid and a generally quiescent melt surface. During the directional solidification, the entire charge, above the interface, was molten and maintained with a superheat of about 250° C. The melt temperature was monitored optically on the top surface and was maintained within ±10° C during the directional solidification.

Both the ingot and the open-end crucible rest on the chill stool and are drawn through the water-cooled copper

chill ring by lowering the stool at a selected, constant rate. The charge is cooled by radiation from the crucible surface to the cold surface of the chill ring. Since heat was constantly removed at the bottom of the crucible by the chill ring and stool, the bottom centimeter of the ingot was not melted. The first material to liquify and then solidify provided an effective seal against the loss of liquid metal. The composite grows epitaxially from the unmelted portion portion of the charge ingot.

Although the heat flux lines for this furnace geometry are not generally parallel, as illustrated with Figure 6, and thus the isotherms need not be flat, a flat interface can be maintained by using the proper thickness of insulation between the susceptor and the chill ring. In this manner, the eutectic temperature isotherm can be positioned where the heat flux lines are parallel. The flat interface is desirable since the aligned growth takes place with the fiber oriented normal to the interface, and a curved interface would promote the growth of fibers which converge to or diverge from the axis of the casting. A flat interface promotes the growth of long, parallel reinforcement fibers.

The rate of interface advance was determined on some test bars by measuring the distance between intentionally introduced perturbations in the growth of the fibers. The rate of interface advance was equal to the rate of

withdrawal of the melt from the furnace. A withdrawal rate varying between 0.7 and 3 cm/hr was employed to produce cylindrically shaped test bars 1.25 cm in diameter and cropped to 7.5 cm length. Melting was performed under a dynamic argon atmosphere of 0.2 m^3/hr.

C) Thermal Fatigue

The directionally solidified test bars were thermally fatigued in the apparatus shown in Figure 7. This type of equipment is typically used to simulate the environment of a jet engine and is widely used in the evaluation of turbine alloys. The cylindrically shaped test bars were quickly heated in the blast of a jet burning a mixture of JP-5 grade jet fuel and air at 1650° C at Mach 0.3 and cooled in a blast of room temperature air at Mach 0.7. To assure uniform heating, the sample holder (Figure 7, insert) was rotated in the blast at about 450 rpm. The test bars were heated to 1093° C, held for 15 seconds and cooled to 427° C. The elapsed time for one cycle, calibrated on a test bar with a thermocouple inserted in it, was two minutes. The temperature profile along the length of the test bar at the end of the heating cycle is shown in Figure 8. The equipment was shut down after every 300 cycles and the test bars were allowed to cool to room temperature. They were weighed periodically to determine the erosion rate.

Samples of the scale were removed and analyzed to determine the constituents present.

Some thermal fatigue testing was conducted using slower heating and cooling rates. For these tests, the equipment shown in Figure 9 was employed where the heating and cooling were accomplished by radiation. The test bars, suspended by platinum-rhodium alloy wires, were alternately held in an air atmosphere alumina tube furnace and a water-cooled stainless steel chamber, both of which were 4 cm in diameter. The furnace was maintained at 1125° C and the total time for one cycle between 427-1093° C was about 12 minutes.

D) Mechanical Testing

After cycling, the test bars were ground to a reduced section, shown in Figure 10 and tested in stress rupture under a helium atmosphere, according to ASTM specification E 139. The stress rupture test was more sensitive to detection of the effects of thermal fatigue in the DSE alloys than either the room temperature or hot tensile tests and more closely resembles the service environment of the material. The stress was applied parallel to the fiber orientation and varied from 69-345 MN/m^2. The testing temperature was varied between 704-1204° C.

After a stress rupture failure, the reduction in

area was measured at the fracture surface. The strain rate during testing was monitored using a dial gage mounted on the test rack. To measure the elongation at failure, the test specimen fracture surfaces were fitted together and the total increase in the specimen length was determined. All of this deformation was assumed to have occurred in the reduced section.

Tensile testing was performed with a standard Instron testing machine using the same specimen geometry as in the stress rupture tests. A constant strain rate of 0.02/min was employed and the strain, during testing, was determined from crosshead deflection.

E) Metallographic Examination

Sample preparation for light microscopy consisted of conventional polishing techniques and etching in a solution of 60% HCl, 15% HNO_3, 15% CH_3COOH, 10% H_2O. The etchant was allowed to stand for about five minutes before use until its color changed to bright yellow. For SEM examination, the same polishing techniques were used and the matrix was deep-etched to reveal a representative length of fiber. The same etchant was used at half strength (water diluent) electrolytically at 12 volts. Because of conduction problems of the TaC fibers in the SEM examination, the samples were plated with a thin layer of a gold-palladium alloy.

A JEOLCO JSM-2 SEM was used in the investigation.

Interfiber spacings were obtained by photographing the transverse section at 1000X. The number of fiber sections which fell within an area of known size were counted. The interfiber spacing, defined as the average center-to-center distance, measured in a plane normal to the fiber axis is calculated by computing the square root of the reciprocal of the fiber density as measured from the photograph. This technique provided consistent results, that were accurate to within 4%.

F) Carbide Fiber Extraction

The TaC fibers were extracted from small sample discs about 1 mm thick in a methanol-10% HCl electrolyte[21]. A current density of 80-100 mA per square centimeter of sample area was maintained with a platinum mesh cathode. This extraction technique provided enough fibrous material, scraped from the surfaces of the discs, for x-ray diffraction and arc emission spectrographic examination. The TaC residues were washed in methanol, filtered, and dried for 24 hours at 100° C. To obtain longer lengths of fibers, the entire matrix can be dissolved in a methanol-30% bromine solution.

III. RESULTS AND DISCUSSION

A) Alloy Development and Structure

A pseudo-binary eutectic reaction occurs in the Co-TaC system at 13%* TaC at 1402° C[22]. When directionally solidified, the fibrous nature of the Co-TaC microstructure is evident as illustrated by Figure 11. The predominantly tri-lamellar fibers are oriented in the mixed FCC/HCP cobalt matrix such that the $(111)_{TaC}$, $(111)_{Co,FCC}$, and $(10.1)_{Co,HCP}$ crystallographic directions are parallel to the growth direction. Although the composite is not monocrystalline, the elongated grains are very coarse (2 mm, diameter). A simple Co-TaC alloy is not suitable for thermal fatigue testing because of low oxidation resistance and because of the allotropic transformation in the cobalt matrix. Typically, in cobalt-base superalloys, chromium is added to yield oxidation resistance, and nickel will stabilize the high temperature, FCC, cobalt phase [23]. Alloys containing 15% chromium and various amounts of nickel were directionally solidified and examined. The amount of retained HCP cobalt as a function of the nickel content is

*% refers to weight percent in alloy compositions

shown in Figure 12 and the appropriate calculations to determine the amount of HCP cobalt are listed in Appendix A.

An alloy composition of Co-15Cr-25Ni-13TaC was acceptable for thermal fatigue testing. The alloy chemistry was checked by wet chemical analysis on representative samples and was within ±1.5% of the reported values. The eutectic point in this alloy occurs at 1396 ±8° C at 12.6 ±0.3% TaC. The matrix is fully FCC stabilized and has oxidation-erosion properties similar to the conventionally cast, cobalt-base superalloy, Mar M-509[24]. While the elevated temperature strength is less than that of other more complex TaC reinforced cobalt-base DSE alloys[8,17], it is believed that the effect of thermal fatigue will be similar in other Co-TaC and Ni-TaC DSE systems where the fiber and matrix orientations are the same as those reported here.

The as-cast structure of the Co-15Cr-25Ni-TaC DSE alloy is shown in Figure 13. The single crystal TaC fibers are approximately square in transverse section and have an aspect ratio exceeding 10,000. The $(100)_{TaC}$ and $(100)_{Co}$ crystallographic directions are parallel to the growth direction in this alloy. Precision x-ray lattice parameter determinations on extracted fibers, using the following equation[25], indicates that the FCC fibers have a C/Ta mole

$$C/Ta = 6.398a_o - 27.516 \qquad (a_o \text{ in angstroms})$$

ratio of about 0.91. Lattice parameter determinations were conducted using conventional powder techniques and the data was refined using a computer program HERTA-4[26]. The longitudinal surfaces of the fibers are [110] planes. The fiber spacing varies linearly with the inverse square root of the rate of interface advance, R, as shown in Figure 14.

B) Isothermal Phase Stability

Phase instability at elevated temperatures in some carbide containing superalloys[27,28] and some DSE alloys[29] led to an investigation of the stability of the Co-15Cr-25Ni-TaC DSE on isothermal heat treatments. Small samples (1.25 cm diameter, 0.25 cm thick) were held under an argon cover at the temperatures and times listed in Table IV. Metallographic and x-ray diffraction examination of the DSE alloy samples showed no change in the appearance, structure, or orientation of either the fibers or the matrix. X-ray powder diffraction and arc emission spectrographic examination of the extracted fibers showed no change in the composition or structure of the fibers as a result of the isothermal heat treatments listed in Table IV.

The formation of the embrittling Laves phase, Co_2Ta, has been seen at the TaC-metal interface where TaC had been exposed at high temperatures to Co,Cr alloys[29,30]. In these cases, the materials were not eutectic alloys, but rather,

mechanical mixtures of the TaC-metal systems. Because of the excellent thermodynamic stability of the DSE alloys at elevated temperatures, the formation of other phases near the TaC fibers in the Co-15Cr-25Ni-TaC DSE alloy, was not observed.

C) Stability Under Thermal Cycling

When tested under conditions of thermal fatigue, cobalt-base TaC systems have shown a seemingly anomalous behavior (pg. 3). The structure of the Co-15Cr-25Ni-TaC DSE alloy as a function of thermal cycling between 427-1093° C is indicated in Figure 15. The previously smooth fibers, shown in Figure 13, developed a serrated appearance that increased in magnitude with the number of applied fatigue cycles. Figure 15a illustrates a small degree of serrations after 200 cycles; Figure 15b shows the more fully developed serrations after 2000 cycles; and Figure 15c demonstrates the very severe serrations after 5000 cycles. Increasing the upper cycling temperature to 1200° C will produce the serrated appearance more rapidly than cycling to only 1093° C. As a result, the material cycled for 500 times to 1200° C has an appearance very similar to the material which had been cycled for 5000 times to 1093° C. Material cycled to an upper temperature of 982° C for up to 5000 cycles indicated no formation of serrations. Bibring[16] also reported

no effect for a similar Co,Cr,Ni-TaC DSE alloy cycled to 1000° C for up to 10,000 cycles.

The appearance of the serrated fibers when viewed on a polished and etched longitudinal section in a light microscope, Figure 16, is not unlike that observed by Breinan in figures 7 and 9 in reference 12. Breinan described this type of condition as "fragmented fibers".

Metallographic and x-ray diffraction examination of the cycled material showed no signs of recrystallization or any microstructural changes other than the serrations. The C/Ta ratio was unaffected by thermal cycling. Identical test bars were cycled at a slower rate by radiation heating and cooling. The effects on the structure of the alloy with this type of cycling were identical to that obtained in the burner rig test. Alloys of the same composition, with differing interfiber spacings (2.5 to 6.0 microns), yielded the same type of microstructural behavior when thermally cycled.

D) Mechanical Properties

Room Temperature

The typically low room temperature ductility (< 2%) of most high performance DSE alloys[4,31-33] has caused some concern for their use in gas turbine engines. This low ductility can lead to premature engine failure from foreign

object damage before the engine has reached operating temperature.

A limited amount of tensile testing was performed to determine room temperature properties of the as-cast alloy. Figure 17 illustrates the room temperature stress-strain curve for the Co-15Cr-25Ni-TaC DSE alloy. This type of curve is typical of the cobalt and nickel MC DSE systems. The salient features of the room temperature stress-strain curve are:

a) the change in modulus, where the matrix begins to undergo plastic deformation while the fibers remain elastic;

b) the elongated yield region, where the fibers fracture into small segments throughout the entire gage section;

c) matrix strain hardening; and

d) very high failure strain, typically about 40%.

Also shown on Figure 17 is the appearance of the TaC fibers during testing. Up to the beginning of the elongated yield region, the fibers remain intact. At the onset of yielding the fibers begin to fail, and this fiber-only failure propagates through the entire reduced section much like the formation of Luders bands in steel. At the termination of yielding, all of the fibers in the gage length have been broken into small sections with an aspect ratio of about 4-6 (See Figure 17). When all of the fibers have fractured

into critical length sections, further strain is accommodated by the strain hardening of the ductile matrix until necking and subsequent failure. The room temperature reduction in area is generally about 35%.

Using simple rule of mixtures calculations (Appendix B), the approximate fracture strength of the TaC fibers can be determined. The calculated fracture stress of the TaC fibers in the as-cast Co-15Cr-25Ni-TaC DSE alloy is 9000 MN/m^2, which approaches the theoretical strength of the material. This value is consistent with those obtained by testing single TaC fibers extracted from the superalloy matrix[11,16]. This indicates that the fibers are almost perfect, dislocation-free, single crystals.

Elevated Temperature

Elevated temperature mechanical properties determined in superalloys generally involves stress rupture testing. The stress rupture test better approximates the service to which the alloy will be subjected and was most effective in detecting differences in mechanical properties as a result of thermal cycling. Stress rupture data is most effectively displayed using the technique of Larson and Miller[34]. The applied stress is plotted as a function of

$$(C + \log t)T,$$

where C is a constant, t is the time to failure, and T is the absolute temperature. The value of C is determined by plotting (log t) versus 1/T; C = -(log t) at (1/T) = 0. This has been accomplished in Figure 18 for the as-cast data where C was determined to be 20. This value of C is consistent with that determined for many other metallic systems[34].

The mechanical properties of the as-cast and cycled materials are shown as a Larson-Miller plot in Figure 19 and tabulated in Table V. The absolute magnitudes of the strengths are not as important as the relative strengths since no attempt was made to optimize the mechanical properties by alloying. As shown in Figure 19, the material cycled to 1093° C exhibits an initial loss in rupture life after 200 cycles. After 2000 cycles, the rupture life has been restored almost to the level of the as-cast material. A further increase in the number of thermal fatigue cycles to 5000 leads to a substantial decrease in the elevated temperature mechanical properties.

When the as-cast material was tested in stress rupture, it failed by a shear mechanism at the shoulder of the gage section, as illustrated by Figure 20. Metallographic examination of the as-cast samples indicated that the matrix failed first in shear, and this led to localized fiber failures along the 45° shear lines. This behavior is indicated in Figure 21 where the stress rupture test was

stopped just prior to the anticipated failure time. This indicates that the strength of the composite can be increased by alloy hardening the matrix.

The failure strain of the as-cast alloy, tested in stress rupture, was 2-4% elongation and 5-10% reduction in area. A typical rupture curve for the as-cast material is shown in Figure 22. Because of relaxation of the grips and loading train, during primary creep, accurate strain measurements of initial creep were impossible. The data does show, explicitly, though, that little or no detectable third stage creep occurs. This type of performance is undesirable in alloys used in gas turbine applications.

Material cycled from 427-1093° C for up to 2000 times exhibited a failure mode identical to the as-cast material, indicating that the fibers were still acting as a reinforcement. The 5000 cycle material failed with considerable deformation (Figure 20) on a plane transverse to the loading direction. This observation, along with the reduced mechanical properties, indicated that the badly serrated TaC fibers, obtained by cycling for 5000 times, no longer possess the strength or the integrity to reinforce the matrix.

E) Solubility

The solubility of the matrix components in the

fibers and the fiber components in the matrix was measured to provide an indication of the phase stability of the alloy. Small samples (1.25 cm diameter, 0.05 cm thick) of the Co-15Cr-25Ni-TaC DSE alloy were vacuum encapsulated in Vycor tubes and held for 25 hours at 760, 1093, and 1204° C followed by a rapid water quench. Another set of samples was held at 1204° C for 25 hours and slowly cooled to room temperature. The bulk composition and the extracted fiber composition were determined by arc emission spectroscopy using a recently developed, high precision analytic system[35]. The matrix composition was determined by subtracting the fiber composition from the bulk composition.

The solubility of the matrix components in the TaC fibers was determined to be independent of temperature over the range measured. The amount of cobalt and nickel dissolved in the TaC was 0.1% ±0.1%; the amount of chromium which was dissolved in the TaC was 1.6% ±0.1%. The solubility of the TaC in the matrix varied as shown in Figure 23. The solvus was seen to increase with temperature from 0.4% at room temperature to 2.2% at 1200° C.

F) Effect of Alloy Chemistry

Attempts were made to decrease the slope of the TaC solvus by alteration of the alloy chemistry. The addition of 4% tantalum (in excess of the 12.2% needed to form the

13% TaC) was made to the matrix and was ineffective in reducing the degeneration of the structure and properties. Although molybdenum has been shown to lower the thermal expansion coefficient of some superalloys[36], the addition of up to 5% molybdenum to the matrix of the Co-15Cr-25Ni-TaC DSE did not alter the formation of the serrated fibers. Additions of 1% cerium and yttrium, elements which have limited solubility in both the matrix and fibers, were tried. It was hoped that these rare earth additions would form a diffusion barrier at the fiber-matrix interface. Alloys with cerium or yttrium showed no change in the formation of the serrated fibers with thermal cycling. The cerium and yttrium additions did affect the oxidation characteristics as described below.

A fully stabilized alloy containing iron (Co-15Cr-7.5 Ni-7.5Fe-TaC) was subjected to thermal fatigue. This alloy developed fiber serrations on thermal cycling which appeared identical to those in the base alloy without iron. The strength, after 2000 cycles, of the iron-containing alloy exceeded that of the as-cast iron-containing alloy by about one Larson-Miller parameter. This type of behavior is similar to that which has been reported for the alloy Co50B3W.

G) Oxidation-Erosion Properties

The alloy additions which provide the superalloys with their high temperature strength generally lowers the resistance of the material to oxidation and sulfidation at elevated temperatures. Even though turbine airfoil sections in use above 1000° C are generally protected by various types of surface coatings[37], resistance to surface degradation is necessary in the event of a coating flaw or failure.

The oxidation-erosion rates of several TaC reinforced DSE alloys were determined by intermittent weighings during the thermal fatigue testing. The results are listed in Table VI. As expected, increasing the maximum cycling temperature produced an increase in the weight loss rate. Additions of cerium reduced the rate while the yttrium additions markedly increased rate and produced a very mottled surface oxide. Stabilization with iron increased the rate and the addition of excess tantalum only slightly increased the erosion rate.

The oxide constituents were determined by x-ray diffraction from scale scraped from the surface of the test bar. The powder pattern data for reflections whose intensity exceeded 5% of the intensity of the strongest line and their interpretation, using ASTM Card File data, are listed in Table VII.

Typical of many superalloys of similar compositions, the chromium has oxidized to α-Cr_2O_3 [38]. The reaction of the cobalt-nickel monoxide with the Cr_2O_3 produces the chromate spinel according to the reaction equation:

$$(Co,Ni)O + C_2O_3 \longrightarrow (Co,Ni)Cr_2O_4.$$

The relative concentrations of the cobalt and nickel in the monoxide and spinel phases is approximately in proportion to their concentrations in the matrix. The tantalum, consistent with the pentavalent metals, oxidizes either to the tri-rutile structures, MTa_2O_6 where M is cobalt or nickel, or Ta_2O_5. The MTa_2O_6 and Ta_2O_5 structures are almost identical. No indication of internal oxidation or preferential attack along the TaC fibers away from the exposed surfaces exists.

IV. INTERPRETATION OF RESULTS

Walter and Cline[39] have demonstrated that the easy growth faces for TaC fibers in a stabilized Co,Cr,Ni matrix to be [111] type and the fiber faces exposed to the matrix are [110]. Thus, since the solubility of the fiber components in the matrix increases with temperature, thermal cycling could produce a cyclic transport of fiber material over the fiber-matrix interface. At elevated temperatures, the matrix will dissolve TaC from the fibers and reprecipitate this material back onto the exposed fiber surface at lower temperatures. Since the easy growth planes for the TaC phase are not coincident with the exposed fiber faces, the TaC which is precipitated at lower temperatures may form [111] oriented ledges. This process of solution and reprecipitation on thermal cycling could result in a serrated appearance similar to that seen in Figure 15.

As the fibers become more serrated and the number of thermal fatigue cycles is increased, the fibers will introduce a dislocation structure into the matrix immediately surrounding the fiber. This behavior has been noted by Benz[17] using transmission electron microscopy. The thermal expansion coefficient mismatch strains push dislocations into the matrix at the jagged fiber ribs. Thus, as the

thermal cycling increases, the matrix becomes stronger from the localized strain hardening around the fibers. At some point the serrations or notches become so severe that the strength of the fibers decreases considerably. If a DSE alloy whose matrix had been strengthened by alloying (Co50B3W for example) is thermally cycled, it is anticipated that initial cycling will increase the mechanical properties above the as-cast values because of the strain hardening of the matrix. Further cycling, in this type of material, will lead to an ultimate loss in properties when the serrated fibers are significantly weakened. As the maximum cycling temperature is lowered, the serrated appearance and the loss of mechanical properties decreases because of the lower solubility difference and reduced atomic mobility at lower temperatures.

One other DSE alloy has been tested under conditions of thermal fatigue[20]. The microstructure consists of lamellae of δ, Ni_3Nb in a nickel-base, γ' hardened matrix. On cycling between 400-1120° C (2.1 minute cycle) for 3000 times, the following was reported[20]:

a) a slight decrease in the elevated temperature properties;
b) coarsening of the γ' precipitate in the matrix; and
c) no microstructural damage to the Ni_3Nb reinforcement phase.

The thermal expansion coefficient mismatch in the γ/γ'-δ

DSE alloy ($\Delta\alpha = 7.5 \times 10^{-6}/^{o}C$) is less than that for the TaC reinforced DSE materials ($\Delta\alpha = 12 \times 10^{-6}/^{o}C$). More important is the fact that in the Ni_3Nb lamellae, the easy growth plane and the lamellar surface exposed to the matrix ($[100]$) are coincident. Although this alloy may have a sloping solvus, as seen in the TaC reinforced DSE alloys, solution and reprecipitation on thermal cycling does not present a problem since no morphological change occurs in the reinforcement as a result of the reprecipitation on thermal cycling.

V. CONCLUSIONS

1. Initial determination of elevated temperature mechanical properties in monocarbide reinforced directionally solidified eutectic alloy systems, based on the Co-15Cr-25Ni-TaC alloy examined, has been encouraging. At temperatures above 1100° C, the rupture properties exceeded all conventional superalloys and aligned eutectic alloys which are being considered for future first stage turbine application.
2. While these types of monocarbide reinforced aligned eutectic alloys do exhibit considerable promise for future gas turbine engine applications, the alloys are, at the present time, limited by microstructural stability problems under conditions of thermal fatigue. The alloy suffers degradation in structure and mechanical properties when undergoing thermal fatigue. The degradation increases with the maximum cycling temperature and number of cycles.
3. This degradation in properties is a result of the solubility differences of the TaC in the matrix as a function of temperature. Serrations are formed on the easy growth planes of the TaC fibers during thermal cycling by solution and reprecipitation of the TaC. During

this thermal cycling, the matrix is strain hardened by the thermal expansion coefficient mismatch. These two opposing effects produce an initial decrease in the stress rupture properties after a few thermal cycles, followed by an improvement in properties after an intermediate number of cycles, with a marked loss in strength after a large number of thermal fatigue cycles.

4. The solubility of the TaC in the matrix increased with temperature from 0.4% at room temperature to 2.2% at 1200° C. The solubility of the matrix constituents in the fibers did not vary with temperature.

5. Variations in the thermal fatigue heating-cooling rate, interfiber spacing, and alloy chemistry were ineffective in preventing or reducing the microstructural degradation. Isothermal treatments at temperatures up to 0.88 T_m produced no change in the structure or properties of the alloy.

VI. REFERENCES

1. The Aircraft Gas Turbine Engine and Its Operation, Pratt and Whitney Aircraft Co., East Hartford, Conn., 1970.

2. S. S. Manson: "Directions in Materials Research Dictated by Stringent Future Requirements," NASA, TM X-67885, Washington, D.C., 1971.

3. F. R. Mollard, M. C. Flemings: "Growth of Composites from the Melt, Part I," Trans. AIME, 1967, vol. 239, pp. 1526-1533.

4. F. D. Lemkey: "Directionally Solidified Eutectic Superalloys," in Metal-Matrix Composites, ed. L. Broutman and R. Krock, Academic Press, New York, 1973.

5. H. Bibring, G. Seibel, M. Rabinovitch: "Nouveaux développements dans l'étude des superalliages à fibres obtenus par solidification dirigée," Mem. Sci. Rev. Met., 1972, vol. 69, pp. 341-358.

6. F. D. Lemkey, E. R. Thompson: "Nickel and Cobalt Eutectic Alloys Reinforced by Refractory Metal Carbides," Met. Trans., 1971, vol. 2, pp. 1537-1544.

7. V. M. Patarini, T. Z. Kattamis: "Structure and Mechanical Behavior of Directionally Solidified Co-NbC Eutectic Alloy," Proc. Conf. In-situ Composites, vol. II, pp. 187-200, NMAB, Washington, D.C., 1973.

8. H. Bibring, J. Trottier, M. Rabinovitch, G. Seibel: "Solidification unidirectionelle d'alliages Co-Cr et Ni-Cr renforcés par des fibres monocristallines de TaC. Structure et proprietes," Mem. Sci. Rev. Met., 1971, vol. 68, pp. 23-41.

9. M. G. Benz, et al: "Exploratory Development for Synthesis and Evaluation of Directionally Solidified Composites for High Temperature Application," General Electric Co., Schenectady, N. Y., Interim Technical Report SRD-72-124, Contract No. F33615-72-C-1870, Air Force Systems Command, Air Force

Materials Lab., Wright-Patterson AFB, Ohio, September, 1972.

10. M. F. Henry: "Tensile and Fracture Behavior of a Ni(Cr)-TaC Fibrous Eutectic," Proc. Conf. In-situ Composites, vol. II, pp. 173-186, NMAB, Washington, D. C., 1973.

11. E. R. Buchanan, L. A. Tarshis: "Carbide-Rod Reinforcement in a Directionally Solidified Nickel-Base Eutectic Alloy," General Electric Co., 71-C-168, Schenectady, N. Y., 1971.

12. E. M. Breinan, E. R. Thompson, F. D. Lemkey: "The Effect of Thermal Cycling on High Temperature Eutectic Composites," Proc. Conf. In-situ Composites, vol. II, pp. 201-222, NMAB, Washington, D. C., 1973.

13. H. K. Richards: "Thermal Expansion of Uranium and Tantalum Moncarbides Up to 2700° C," Nuc. Tech., 1971, vol. 10, pp. 54-61.

14. C. A. Hoffman: "Effects of Thermal Loading on Composites with Constituents of Differing Thermal Expansion," NASA, TN D-5926, Washington, D. C., 1970.

15. E. Scala: "Design and Performance of Fibers and Composites," in Fiber Composite Materials, p. 131-156, ASM, Cleveland, Ohio, 1964.

16. H. Bibring: "Mechanical Behavior of Unidirectionally Solidified Composites," Proc. Conf. In-situ Composites, vol. II, pp. 1-69, NMAB, Washington, D. C., 1973.

17. M. G. Benz, et al: "Exploratory Development for Synthesis and Evaluation of Directionally Solidified Composites for High Temperature Application," General Electric Co., Schenectady, N. Y., Interim Technical Report SRD-72-172, Contract No. F33615-72-C-1870, Air Force Systems Command, Air Force Materials Lab., Wright-Patterson AFB, Ohio, December, 1972.

18. H. E. Collins: "Development of High Temperature Nickel Base Alloys for Jet Engine Turbine Bucket Application," NASA, Cr-54507, Washington, D. C., 1967.

19. B. J. Piearcey, F. L. VerSnyder: A New Development in Gas Turbine Materials. The Properties and Characteristics of PWA 664, Pratt and Whitney

Aircraft Co., East Hartford, Conn., 1965.

20. F. D. Lemkey: "Eutectic Superalloys Strengthened by δ, Ni_3Cb Lamellae, and γ', Ni_3Al Precipitates," United Aircraft Research Lab., Report UARL M911213-15, Contract NAS 3-15562, NASA, Lewis Research Center, Cleveland, Ohio, 1973.

21. M. J. Donachie, O. H. Kriege: "Phase Extraction and Analysis in Superalloys," J. of Mat., 1972, vol. 7, pp. 269-278.

22. H. Bibring, G. Seibel: "Cristallisation orientée dans le système cobalt-tantale-carbone," Compt. Rend., 1969, vol. 268, pp. 144-147.

23. Cobalt-Base Superalloys - 1970, Centre d'Information du Cobalt, Brussels, 1970.

24. J. R. Johnston, R. L. Ashbrook: "Oxidation and Thermal Fatigue Cracking of Nickel- and Cobalt-Base Alloys in a High Velocity Gas Stream," NASA, TN D-5376, Washington, D. C., 1969.

25. A. L. Bowman: "The Variation of Lattice Parameter with Carbon Content of Tantalum Carbide," J. Phys. Chem., 1961, vol. 65, pp. 1596-1598.

26. R. E. Vogel, C. P. Kempter: "A Mathematical Technique for the Precision Determination of Lattice Parameters," Acta Cryst., 1961, vol. 14, pp. 1130-1134.

27. H. E. Collins: "Relative Long Time Stability of Carbide and Intermetallic Phases in Nickel Base Superalloys," Trans. ASM, 1969, vol. 62, pp. 82-104.

28. J. L. Walter, H. E. Cline: "Stability of the Directionally Solidified Eutectics NiAl-Cr and NiAl-Mo," Met. Trans., 1973, vol. 4, pp. 33-38.

29. B. Botic, W. R. Spenser, W. F. Stuhrke: "Thermophysiochemical Campatibility Between Metal Carbides and Metal Matrices," Air Force Materials Lab., Report AFML-TR-71-134, Wright-Patterson AFB, Ohio, 1971.

30. I. Ahmad, J. M. Barranceo, K. E. Loomis, W. J. Heffernan: "Metal Matrix Composites for High Temperature Application," U. S. Army Weapons Command, Report WVT-7155, Watervliet Arsenal,

Watervliet, New York, 1971.

31. J. L. Walter, H. E. Cline: "The Effect of the Solidification Rate on Structure and High Temperature Strength of the Eutectic NiAl-Cr," Met. Trans., 1970, vol. 1, pp. 1221-1229.

32. E. R. Thompson, F. D. Lemkey: "Structure and Properties of Ni_3Al (γ') Eutectic Alloys Produced by Unidirectional Solidification," Trans. ASM, 1969, vol. 62, pp. 140-154.

33. R. Kossowsky, W. C. Johnston, B. J. Shaw: "Mechanical Properties of Unidirectionally Solidified Ni-Cr Eutectic," Trans. AIME, 1969, vol. 245, pp. 1219-1225.

34. F. R. Larson, J. Miller: "A Time-Temperature Relationship for Rupture and Creep Stresses," Trans. ASME, 1952, vol. 74, pp. 765-775.

35. W. A. Gordon, G. B. Chapman: "Quantitative Direct Current Arc Analysis of Random Composition Microgram Residues in a Silver Chloride Common Matrix," NASA, TN D-5532, Washington, D. C., 1969.

36. H. Morrow, III: "The Effects of Molybdenum and Aluminum on the Thermal Expansion Coefficients of Nickel-Base Alloys," Climax Molybdenum Co., Report RP-57-70-02, Ann Arbor, Mich., 1971.

37. S. J. Grisaffe: "Coatings and Protection," in The Superalloys, ed. C. T. Sims and W. C. Hagel, John Wiley and Sons, New York, 1972.

38. S. J. Grisaffe, C. E. Lowell: "Examination of Oxide Scales on Heat Resisting Alloys," NASA, TN D-5019, Washington, D. C., 1969.

39. J. L. Walter, H. E. Cline: "Morphologies of Refractory Carbides Obtained by Directional Solidification in the Eutectic Systems Ni-TaC, Co-TaC, and Fe-TaC," Proc. Conf. In-situ Composites, vol. I, pp. 61-74, NMAB, Washington, D. C., 1973.

40. S. M. DeCorso, D. E. Harrison: "Ceramics in Industrial Gas Turbines," ASME Report 72-GT-04, 1972.

VII. TABLES

ALLOY	VOLUME PERCENT CARBIDE	MELTING TEMPERATURE °C	SPECIFIC GRAVITY*
Co - HfC	15	----	9.7
Co - NbC	12	1365	8.8
Co - TiC	16	1360	8.5
Co - TaC	10	1402	9.4
Co - VC	20	----	8.3
Ni - HfC	30	1260	10.0
Ni - NbC	11	1328	8.8
Ni - TiC	6	1307	8.7
Ni - TaC	8	1340	9.3

* calculated using rule of mixtures

Table I

Cobalt and Nickel Monocarbide Eutectic Data

MATERIAL	NOMINAL PURITY	SUPPLIER	FORM
carbon	.995	Union Carbide	granules BB7
cerium	.999	American Potash	powder
cobalt	.995	Kulite	electrolytic chips
chromium	.99	Union Carbide	electrolytic chips
iron	.999	Armco	electrolytic chips
nickel	.995	INCO	electrolytic chips
molybdenum	.995	Climax	shavings
tantalum	.996	Wah Chang	roundels
yttrium	.999	American Potash	powder

Table II

Raw Materials Data

PART	MATERIAL	GRADE	SUPPLIER	DIMENSIONS ID x OD x LENGTH (cm)
crucible	alumina	ΔRR	Morganite	1.75 x 1.27 x 20
susceptor	graphite	CS	Union Carbide	1.91 x 3.81 x 20
heat shield	alumina	AV-30	McDanel	4.13 x 4.92 x 20
envelope	fused silica	T-42	Amercil	5.08 x 6.35 x 69
insulator	zirconia			1.91 x 10.2 x 1.27
chill ring	copper			1.893 x 10.2 x 1.6
RF coil	copper			0.64 dia. tubing

Table III

Directional Solidification Furnace Materials and Dimensions

TEMPERATURE °C	TEMPERATURE % T_m	TIME hours
760	62	500
843	67	150, 500
954	74	150, 500, 800
1093	82	100, 500
1149	85	100, 250
1204	88	20, 250

Table IV

Isothermal Heat Treatments

NUMBER OF CYCLES (427-1093°C)	STRESS MN/m^2	TEMPERATURE °C	LIFE hr	$T(20 + \log t)x10^{-3}$ °K, hr		ELONGATION %	REDUCTION IN AREA %	
0	345	704	312	22.0		2.9	6.0	
0	345	760	17	21.9		6.1	20.0	*
0	345	815	5	22.5		8.0	25.4	
0	276	760	2035	24.1		2.4	3.1	
0	276	815	242	24.3		1.6	3.9	
0	276	872	5	23.7		4.1	10.8	
0	241	872	100	25.2		1.6	1.6	
0	241	982	3	25.7		3.0	4.4	
0	207	872	565	26.2		2.9	4.6	
0	207	927	411	27.1		2.1	0.5	
0	207	982	35	27.1		NA	NA	
0	207	1038	4	27.0		3.8	10.2	*
0	172	982	140	27.8		1.2	2.2	
0	172	1038	25	28.0		3.0	2.3	
0	172	1093	3	27.9		11.0	62.4	
0	138	1038	373	29.6		2.1	0.5	*
0	138	1093	85	29.9		NA	NA	
0	138	1149	9	29.8		NA	NA	
0	124	1038	981	30.2		4.0	18.3	
0	103	1093	252	30.6		3.0	3.6	
0	103	1121	102	30.7		2.5	3.9	
0	103	1149	70	31.0		2.0	4.7	*
0	103	1204	15+	31.3+	**			
200	276	815	4	22.4		10.8	34.2	
200	241	872	8	23.9		NA	NA	
200	207	872	43	24.8		4.0	14.6	
200	172	927	7	25.0		1.6	2.5	
200	138	1038	72	28.7		8.3	35.5	
200	138	1093	18	29.1		4.3	10.8	
200	103	1038	1311+	30.3+	**			
2000	276	872	2	23.2		9.2	39.6	
2000	207	927	20	25.4		3.5	2.4	
2000	172	927	1072	27.2		5.9	26.0	
2000	138	982	3811	29.6		4.2	16.0	
2000	138	1038	130	29.0		5.6	16.1	
2000	138	1093	26	29.3		6.6	12.2	
2000	103	1093	121	30.2		5.9	13.3	
2000	69	1093	750	31.3		11.8	62.7	
5000	276	815	3	22.3		17.0	59.0	
5000	207	872	13	24.2		16.5	61.1	
5000	172	927	6	24.9		20.0	76.1	
5000	138	982	235	28.1		10.9	53.2	
5000	138	1038	5	27.1		15.8	84.0	
5000	103	1093	11	28.7		18.2	77.6	

* Held for 100 hrs at 0.88 Tm before testing
** Test not completed

Table V

Stress Rupture Test Data

ALLOY COMPOSITION	CYCLING TEMPERATURES °C	EROSION RATE mg/cm^2/1000 cycles
Co-15Cr-25Ni-TaC	427-1093	37
Co-15Cr-25Ni-1Ce-TaC	"	33
Co-15Cr-25Ni-1Y-TaC	"	90
Co-15Cr-25Ni-4Ta-TaC	"	42
Co-15Cr-7.5Ni-7.5Fe-TaC	"	62
Co-15Cr-25Ni-TaC	427-1200	250

Table VI

Erosion Rates for TaC Reinforced DSE Alloys

experimental		$(Co,Ni)Cr_2O_4$	(Co,Ni)O	α-Cr_2O_3	β-Co	TaC	$(Co,Ni)Ta_2O_6$	CeO_2	Y_2O_3
3.60				3.63					
3.35							3.34		
3.24									
3.15	*							3.12	
3.08	**								3.06
2.94		2.94							
2.71	*							2.70	
2.68				2.67					
2.56						2.57	2.56		
2.52		2.52		2.49					
2.44			2.44						
2.37							2.36		
2.26	**								2.26
2.23						2.23			
2.18				2.17					
2.12			2.11						
2.07		2.08							
2.05				2.03	2.04				
1.91	*							1.91	
1.87	**								1.87
1.82				1.81					
1.78					1.77				
1.76									
1.73							1.74		
1.72		1.71							
1.67				1.67			1.67		
1.62	*							1.63	
1.60		1.60							1.60
1.57						1.57	1.57		
1.49			1.50						
1.47		1.47		1.47					
1.43				1.43					
1.39							1.40		
1.37	*							1.37	
1.35						1.35			
1.27		1.27	1.27						
1.25					1.25				
1.22			1.22						
1.21								1.21	
1.20							1.20		

*found only in Ce alloy
**found only in Y alloy

Table VII

"d" Spacings from Oxide Powder Patterns

VIII. FIGURES

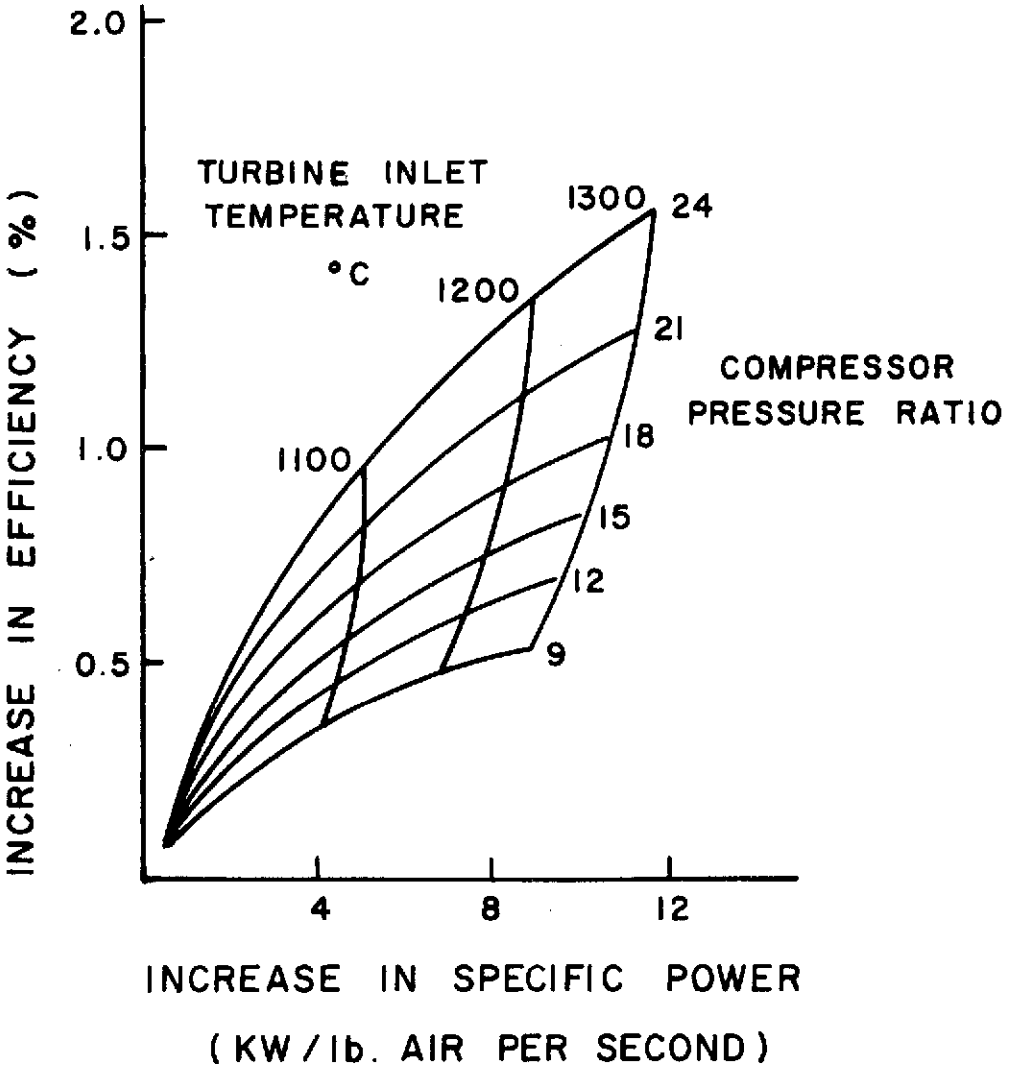

FIGURE 1: INCREASE IN EFFICIENCY OF A GAS TURBINE ENGINE WITH INCREASING TURBINE INLET TEMPERATURE (REFERENCE 40)

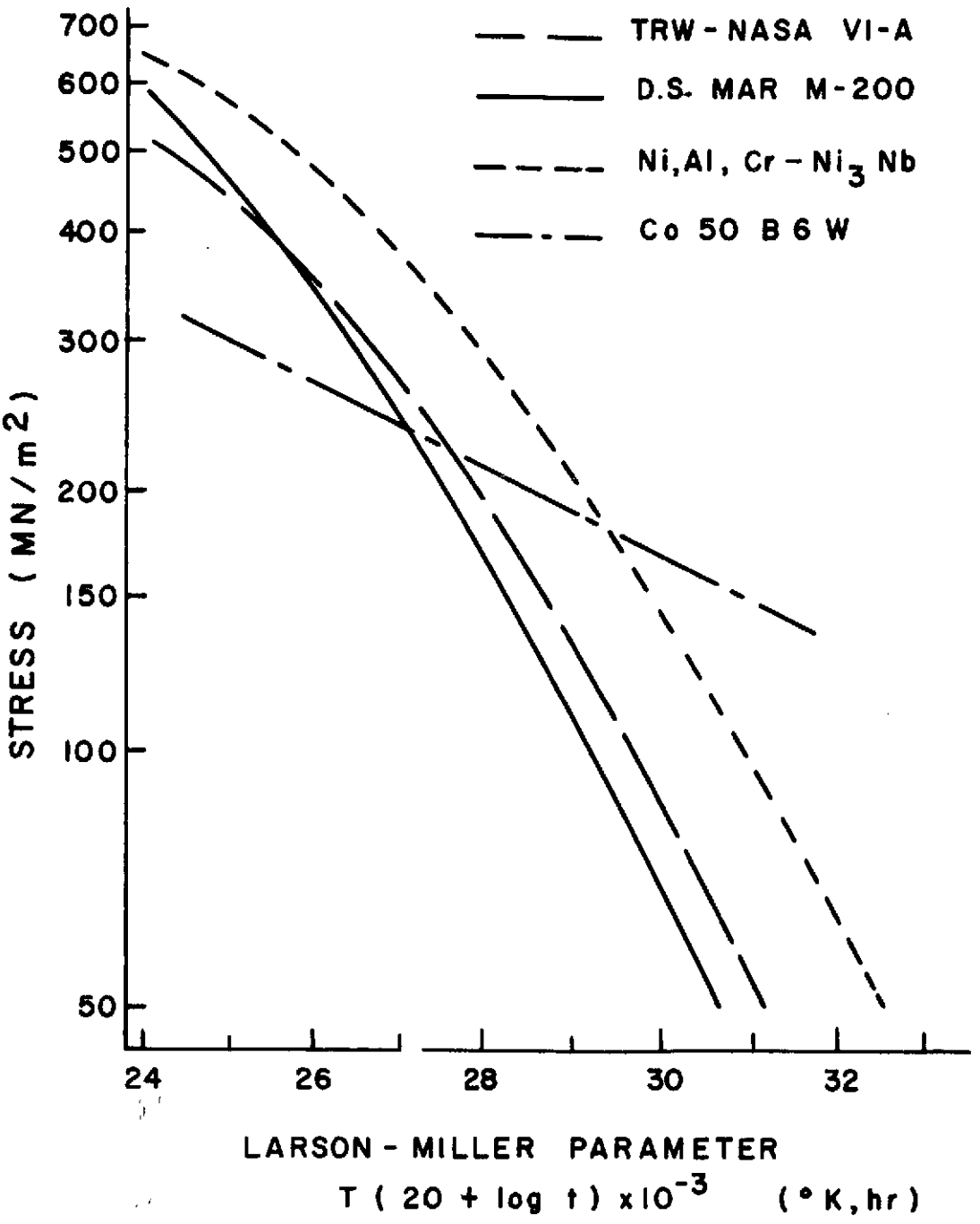

FIGURE 2: COMPARISON OF SUPERALLOY STRESS RUPTURE DATA

FIGURE 3: DIRECTIONAL SOLIDIFICATION FURNACE - PHOTOGRAPH

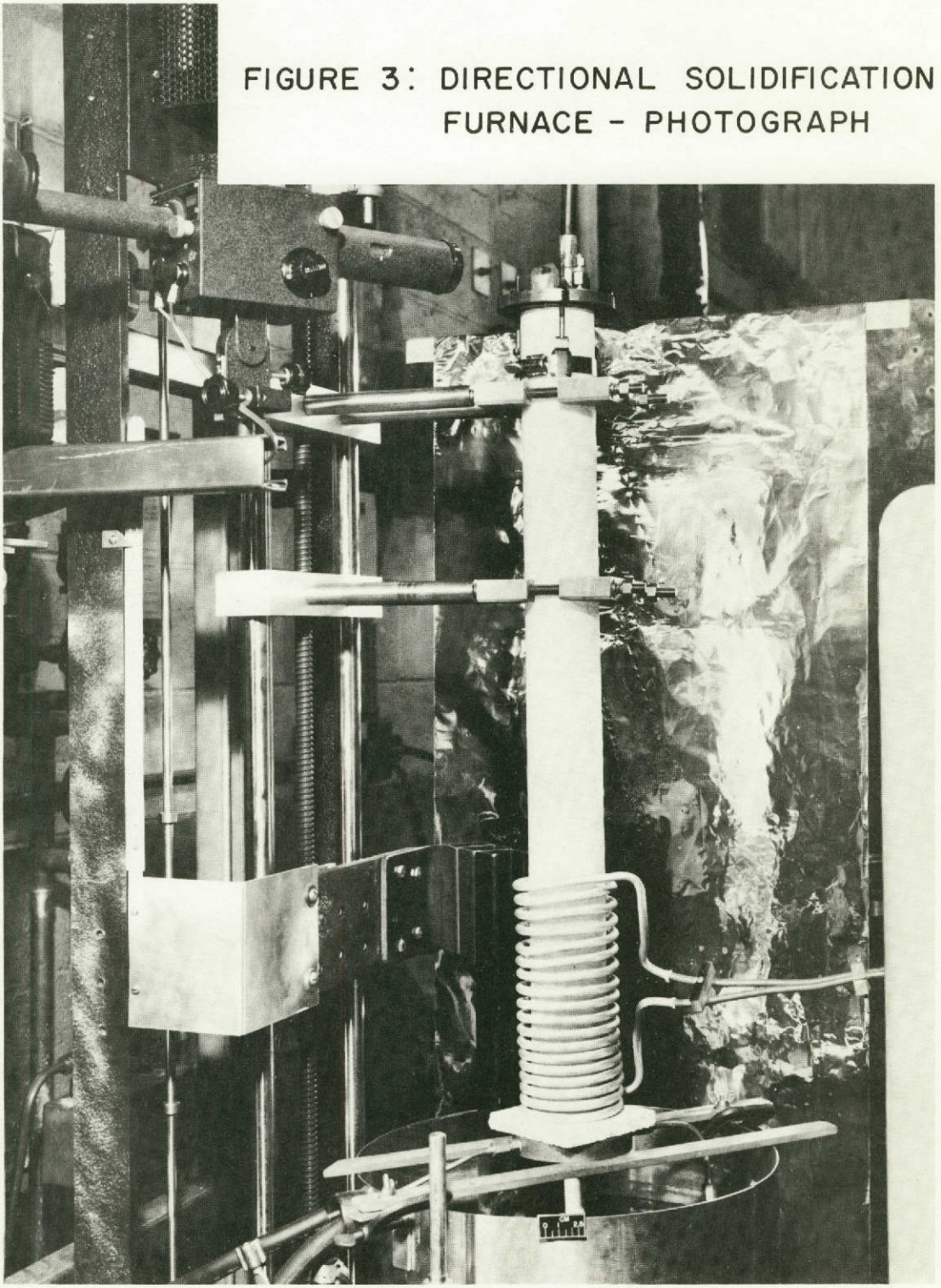

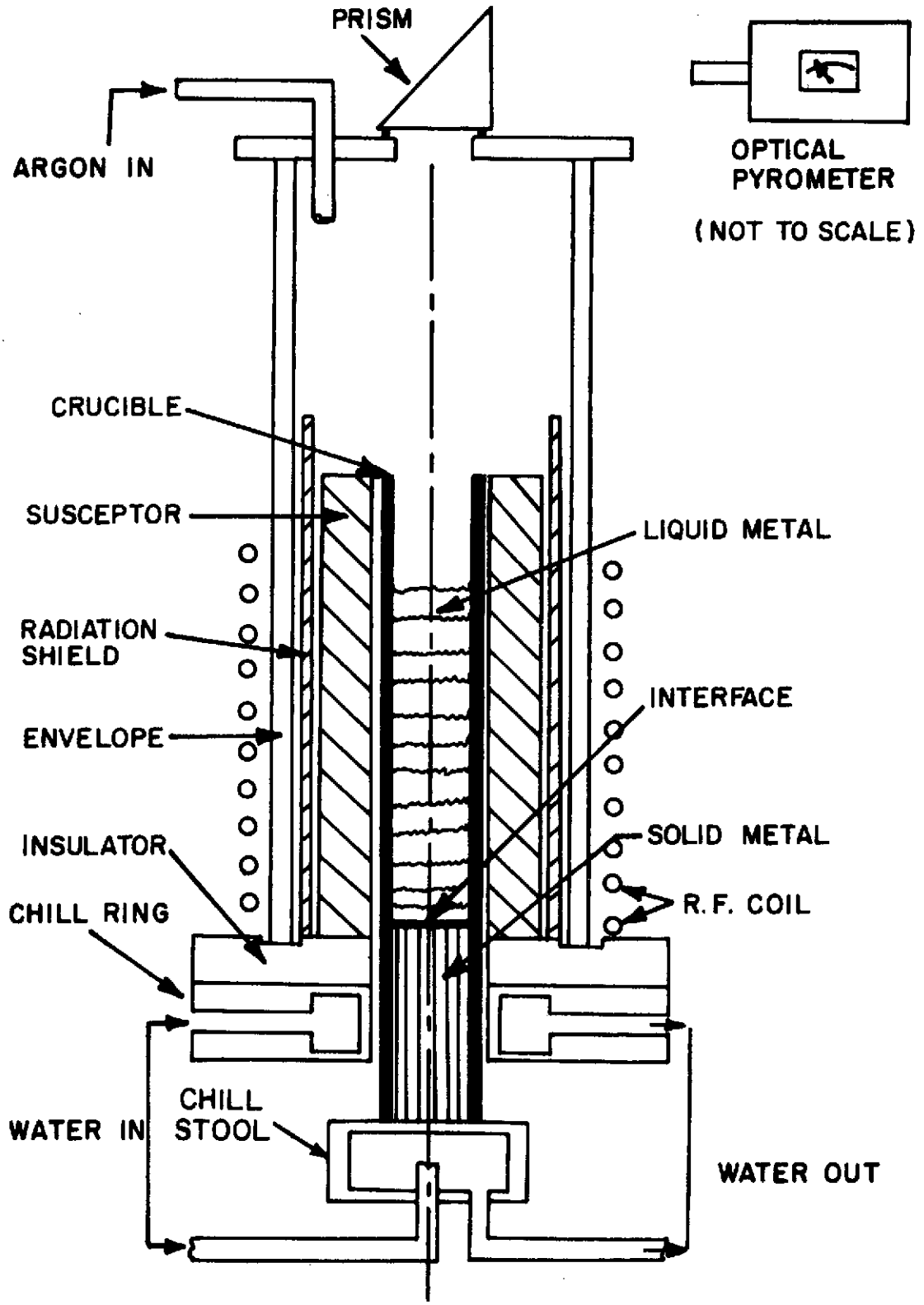

FIGURE 4: DIRECTIONAL SOLIDIFICATION FURNACE - ILLUSTRATION

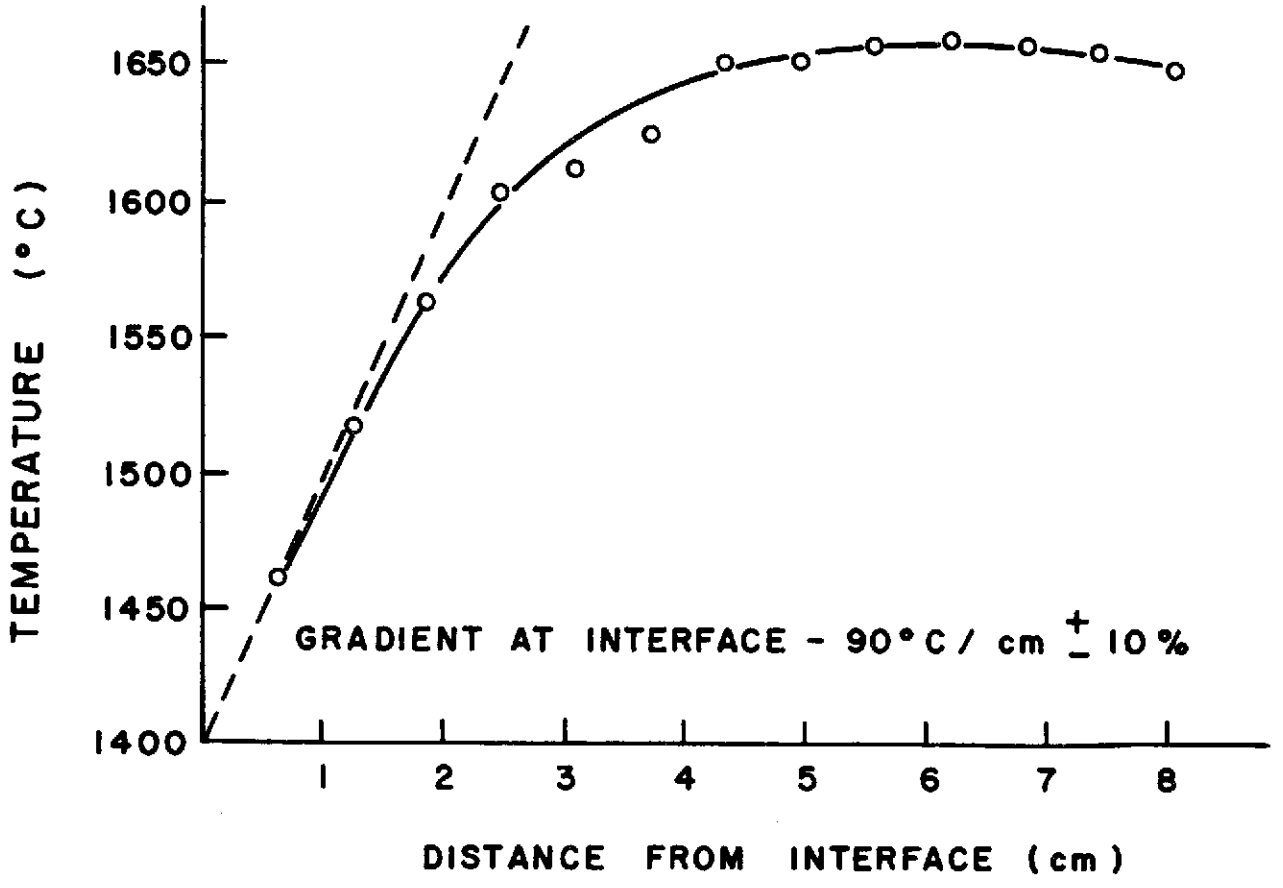

FIGURE 5: TEMPERATURE PROFILE IN LIQUID DURING DIRECTIONAL SOLIDIFICATION

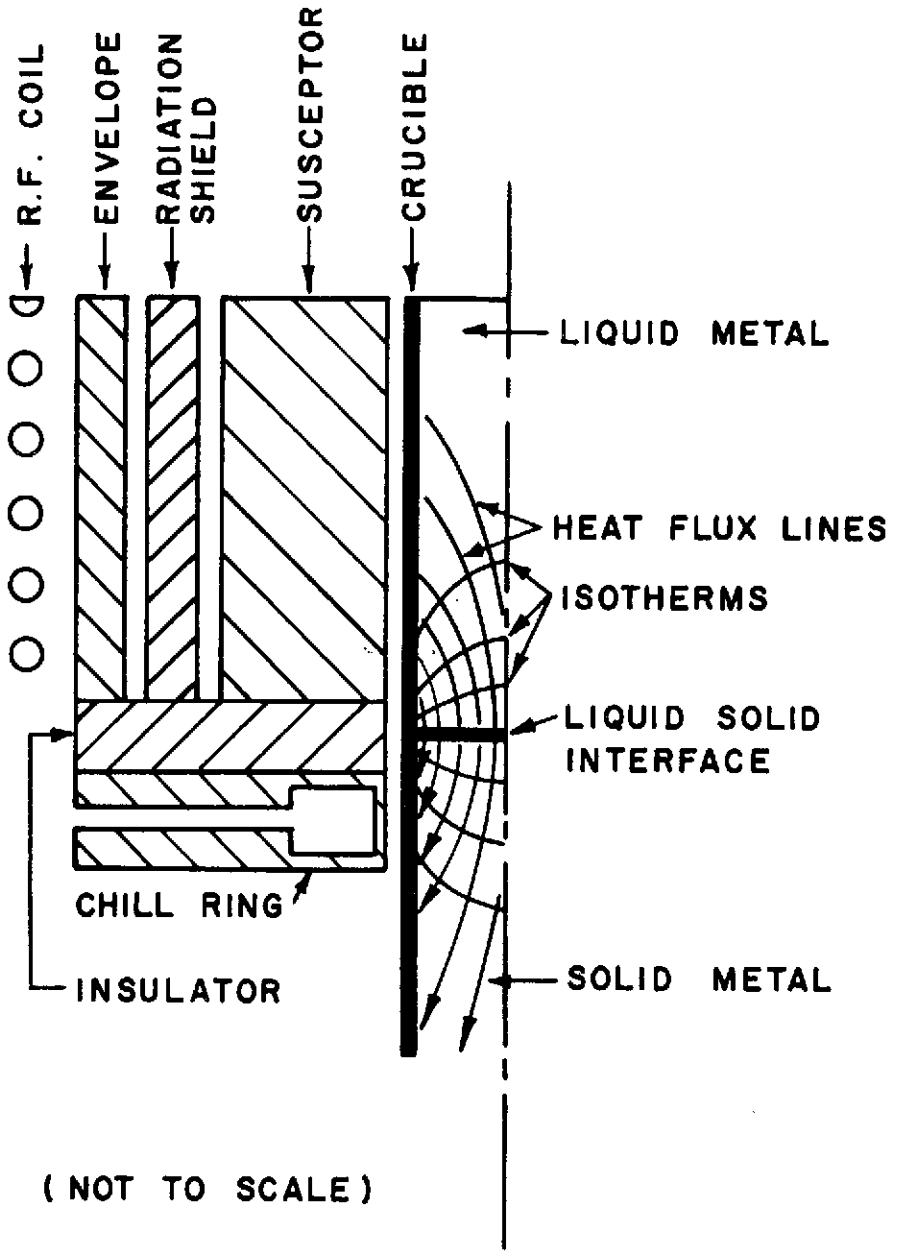

FIGURE 6 : HEAT FLOW DURING STEADY-STATE DIRECTIONAL SOLIDIFICATION

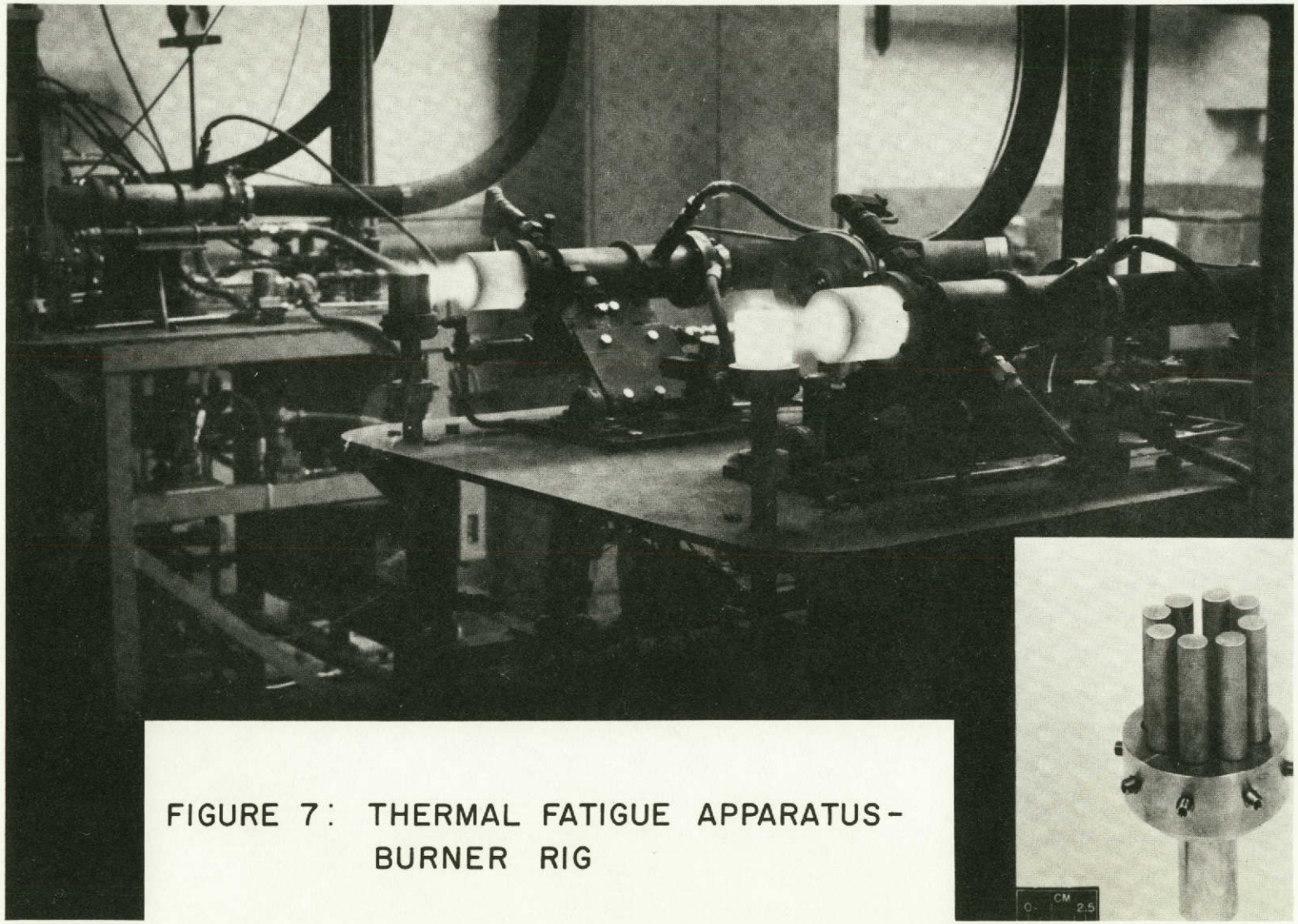

FIGURE 7: THERMAL FATIGUE APPARATUS - BURNER RIG

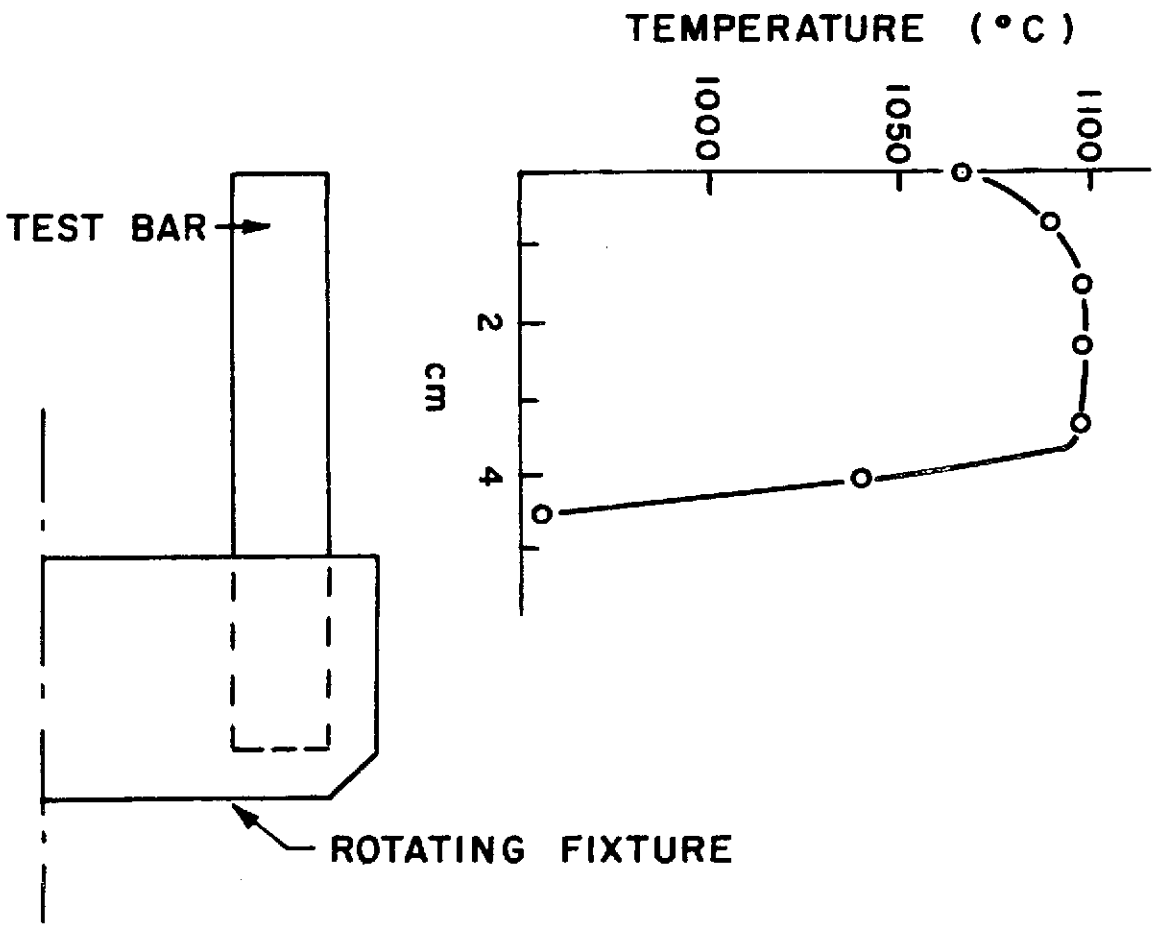

FIGURE 8: TEMPERATURE PROFILE ALONG THERMAL FATIGUE TEST BAR

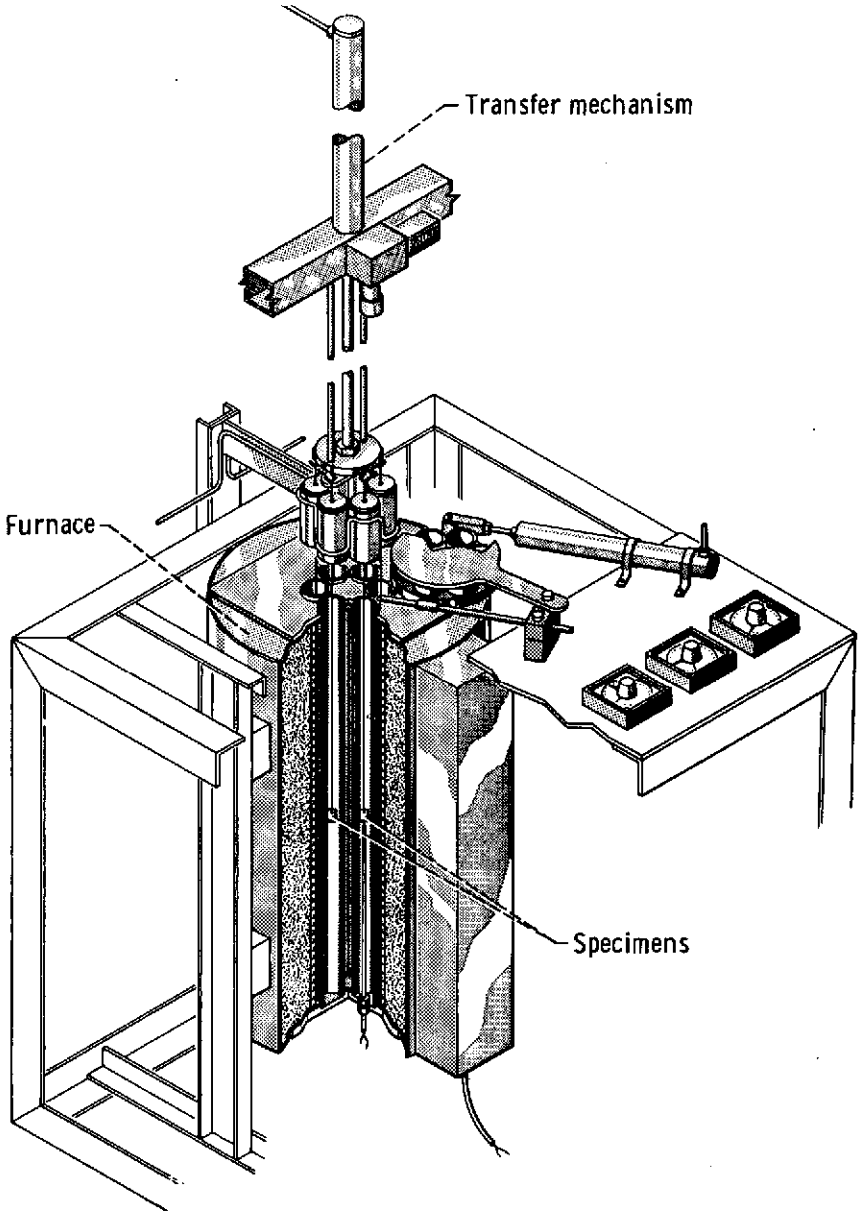

FIGURE 9: THERMAL FATIGUE APPARATUS - RADIATION FURNACE

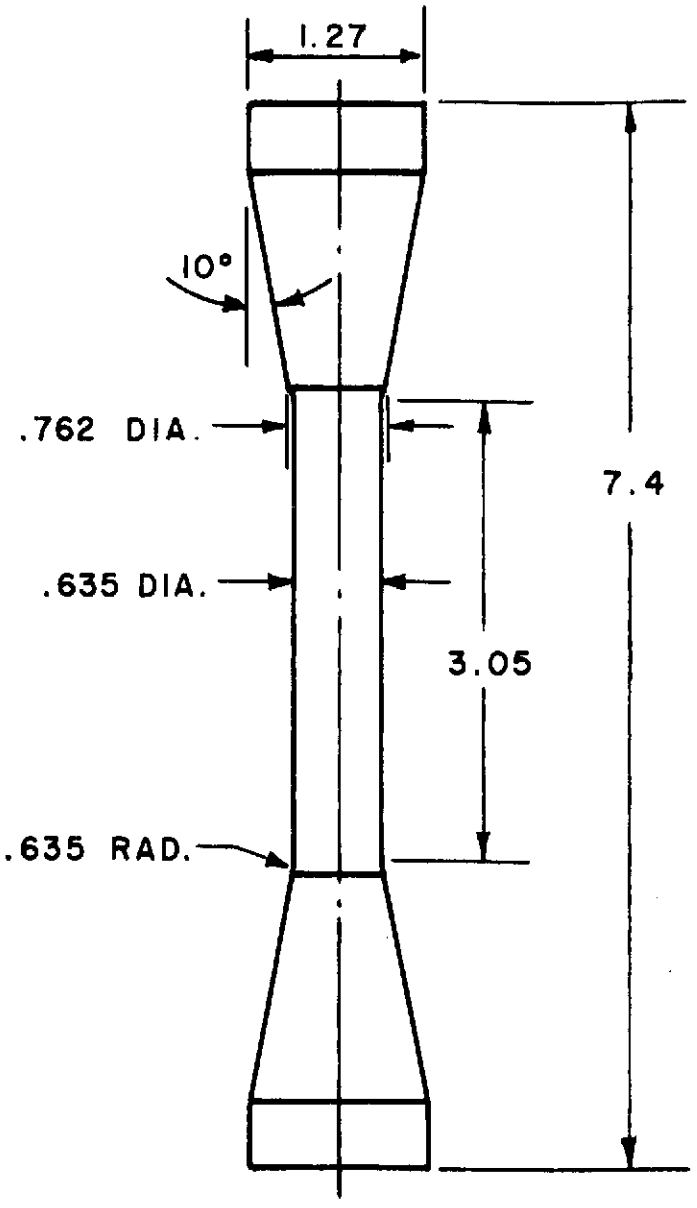

ALL DIMENSIONS IN CENTIMETERS

FIGURE 10: TENSILE - STRESS RUPTURE TEST SPECIMEN GEOMETRY

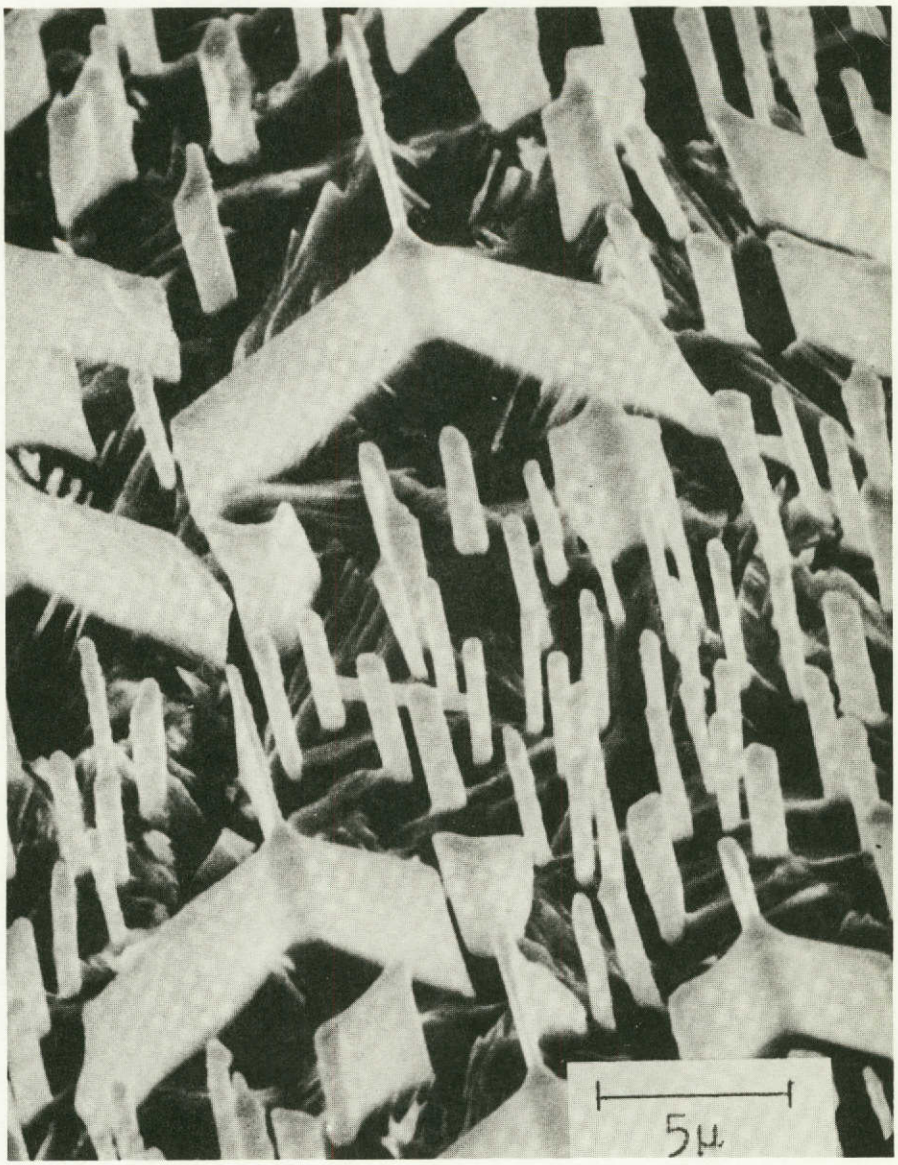

Figure 11: Structure of Directionally Solidified Co-TaC

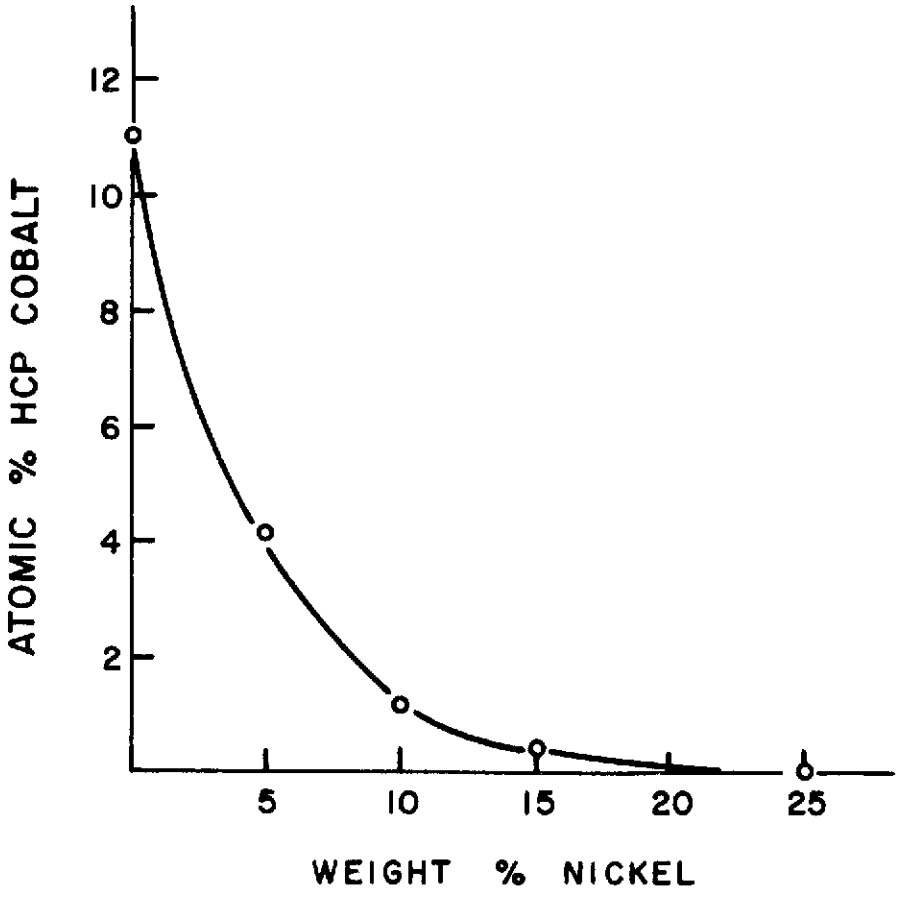

FIGURE 12 : AMOUNT OF HCP COBALT IN THE Co - 15 Cr - XNi MATRIX

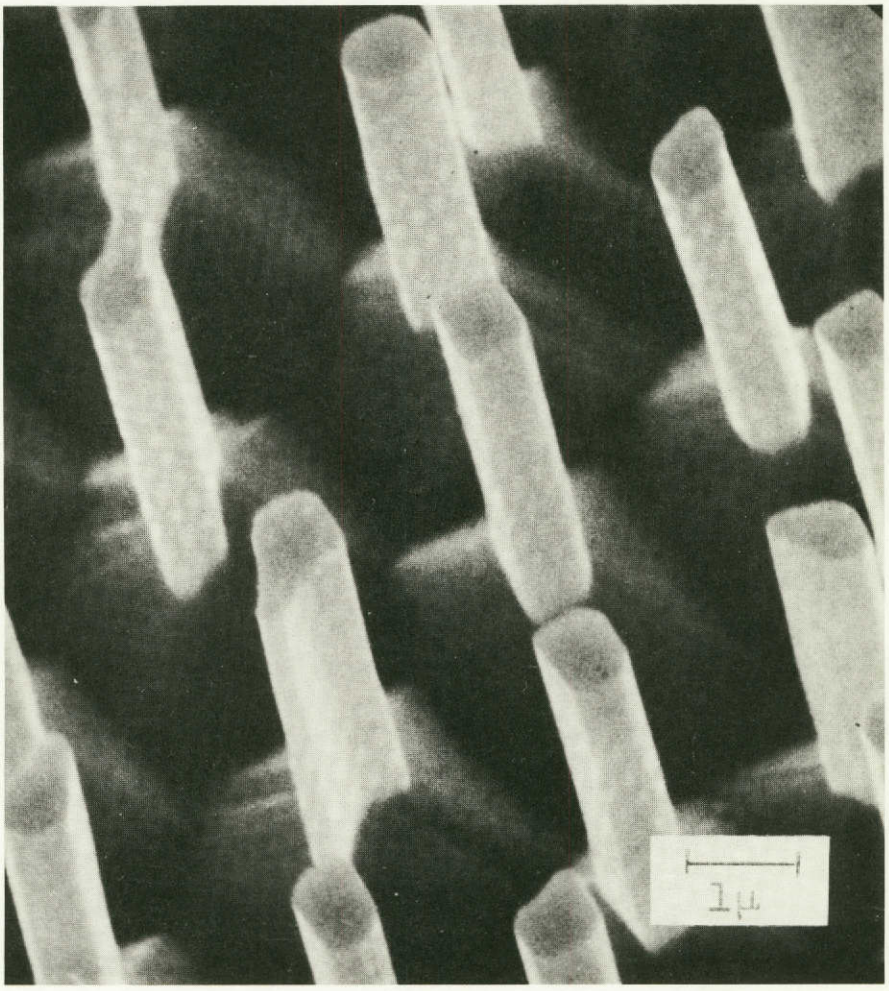

Figure 13: Structure of Directionally Solidified Co-15Cr-25Ni-TaC

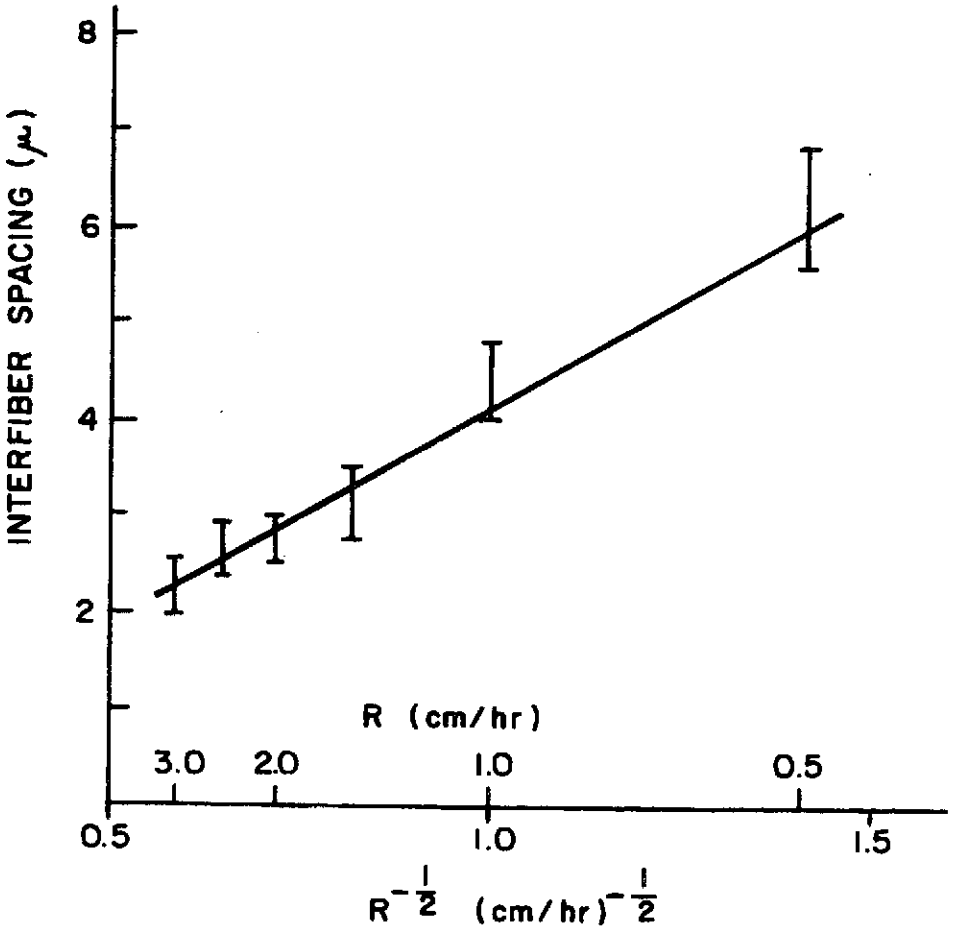

FIGURE 14: VARIATION OF INTERFIBER SPACING WITH RATE OF INTERFACE ADVANCE, R

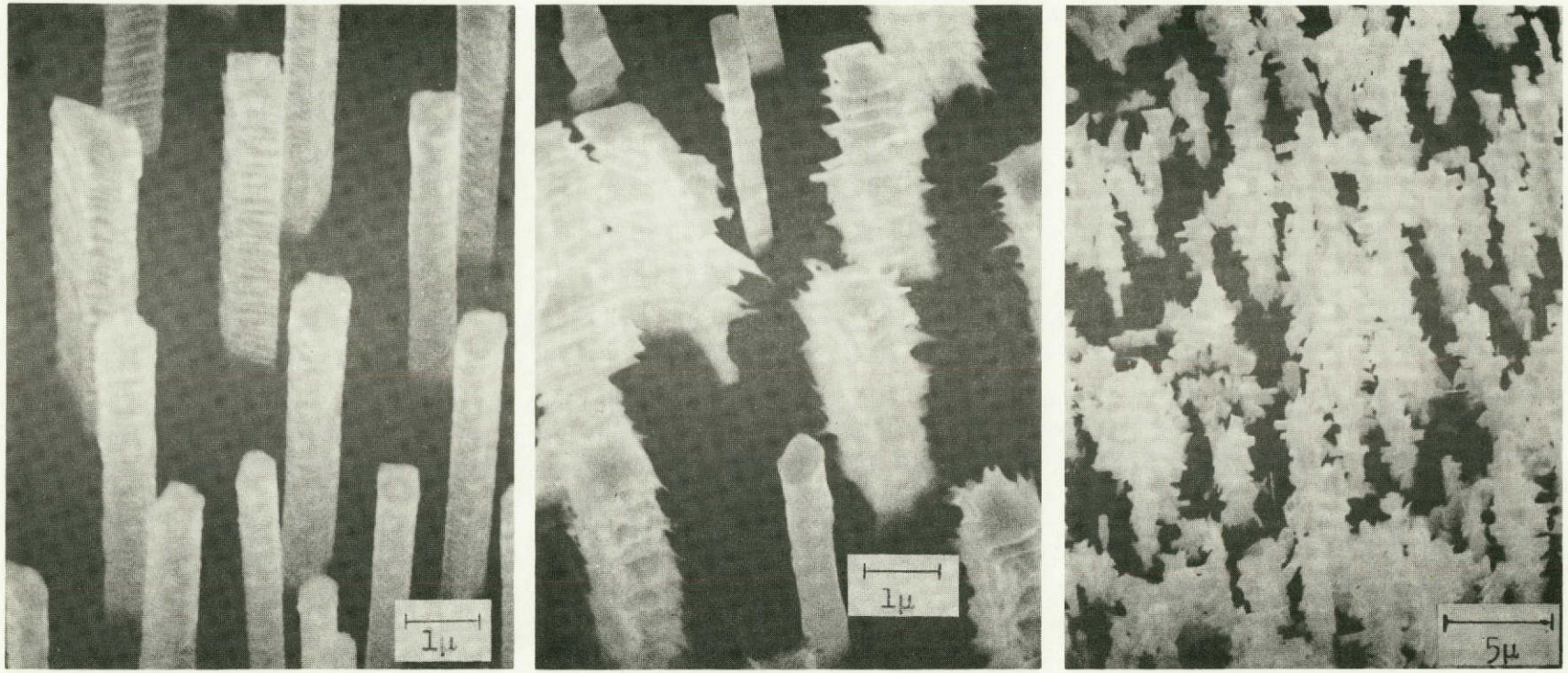

a) 200 cycles b) 2000 cycles c) 5000 cycles

Figure 15: Structure of Thermally Cycled Co-15Cr-25Ni-TaC DSE

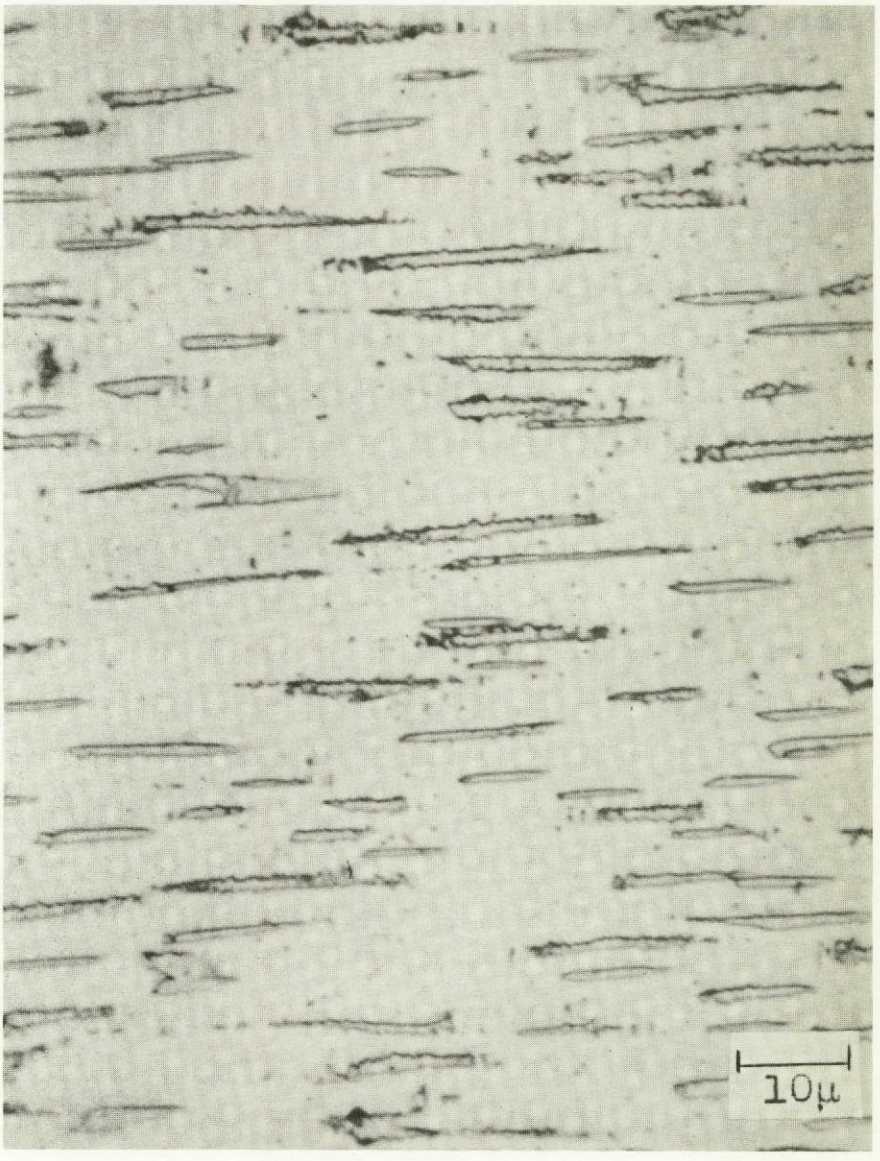

Figure 16: Longitudinal Section of Thermally Cycled Co-15Cr-25Ni-TaC DSE

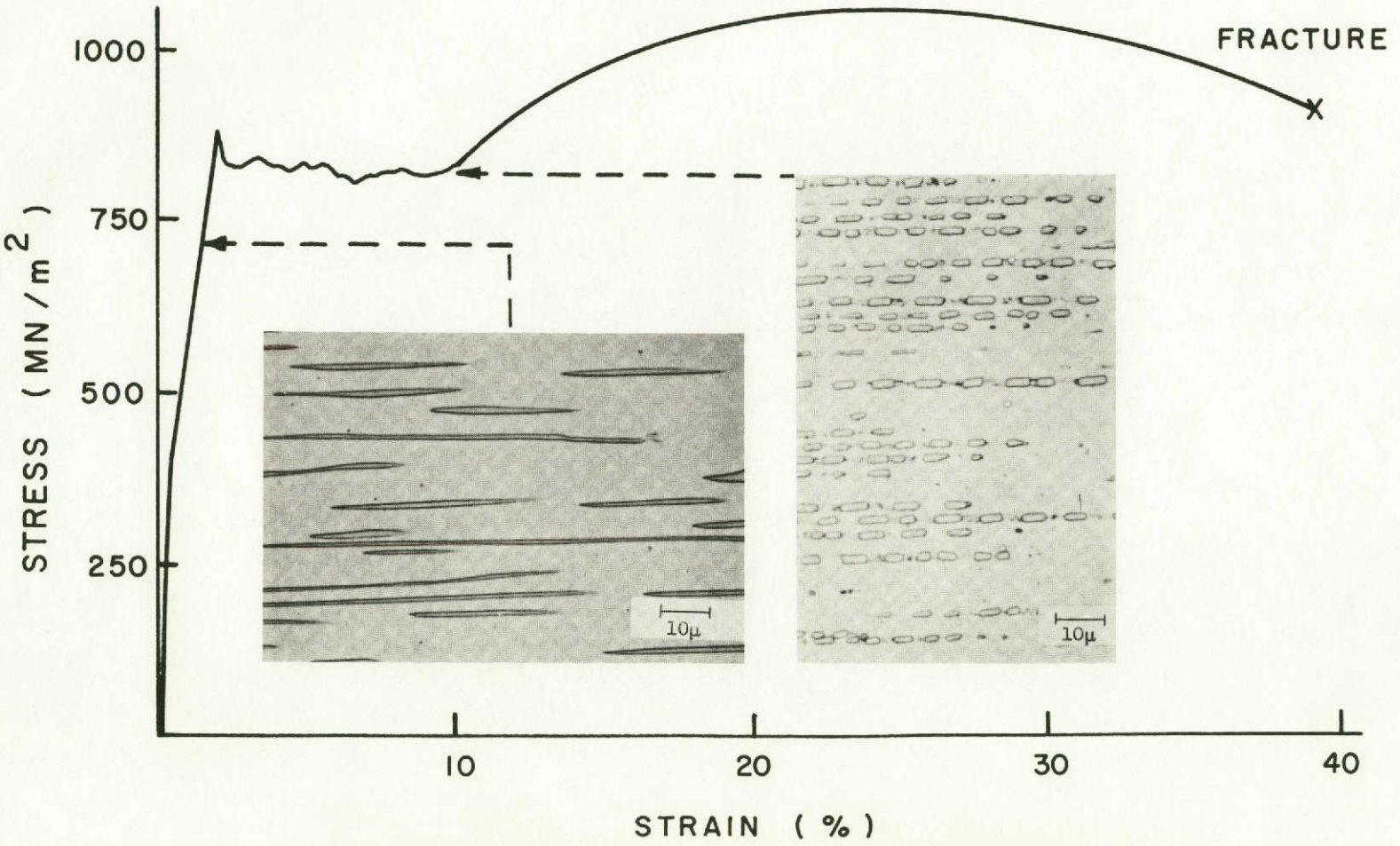

FIGURE 17 : ROOM TEMPERATURE STRESS - STRAIN CURVE

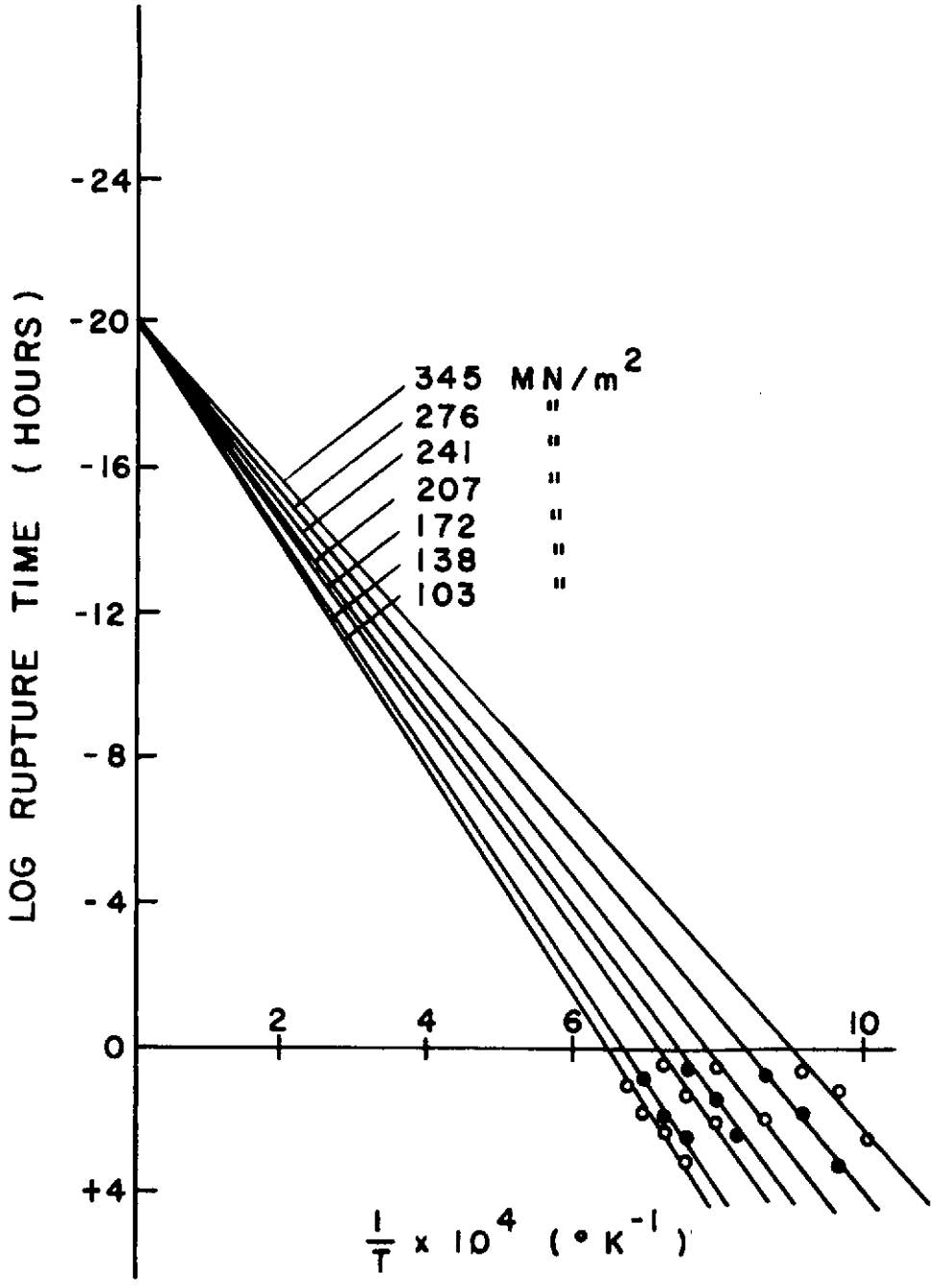

FIGURE 18: LOG RUPTURE TIME VS 1/T FOR AS CAST Co-15 Cr-25 Ni-TaC

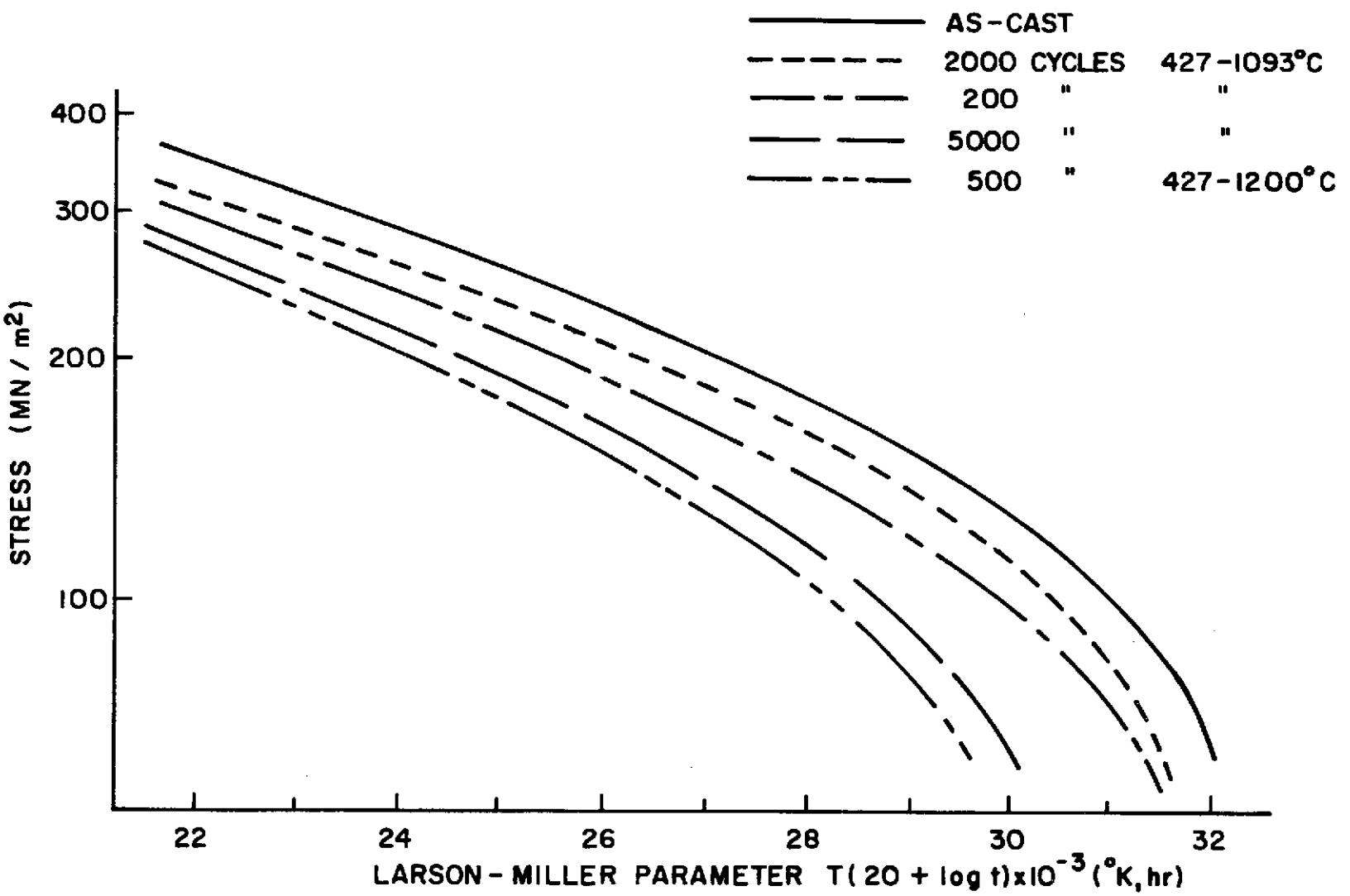

FIGURE 19: ELEVATED TEMPERATURE PROPERTIES OF AS-CAST AND THERMALLY CYCLED Co-15 Cr-25 Ni-TaC DSE

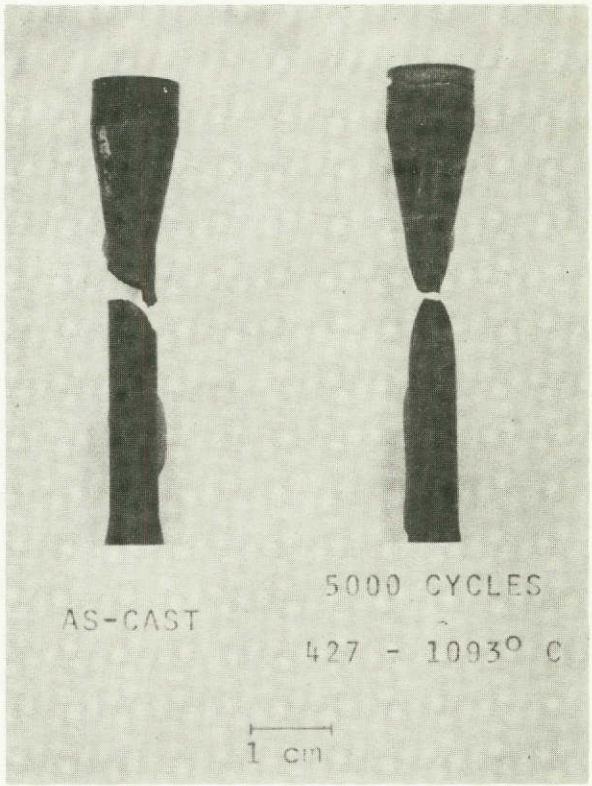

Figure 20: Test Bars Failed in Stress Rupture

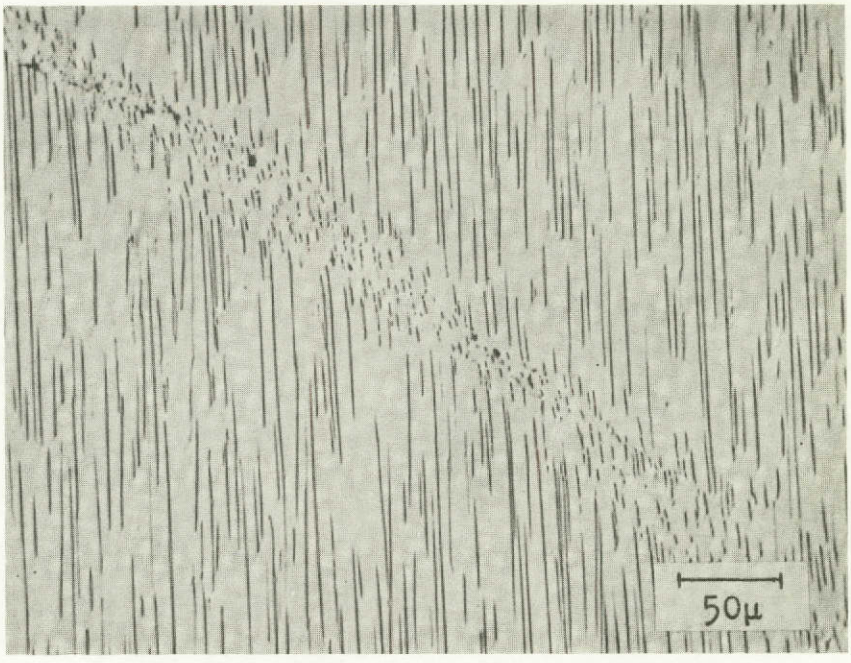

Figure 21: Structure of As-cast Co-15Cr-25Ni-TaC DSE Prior to Stress Rupture Failure

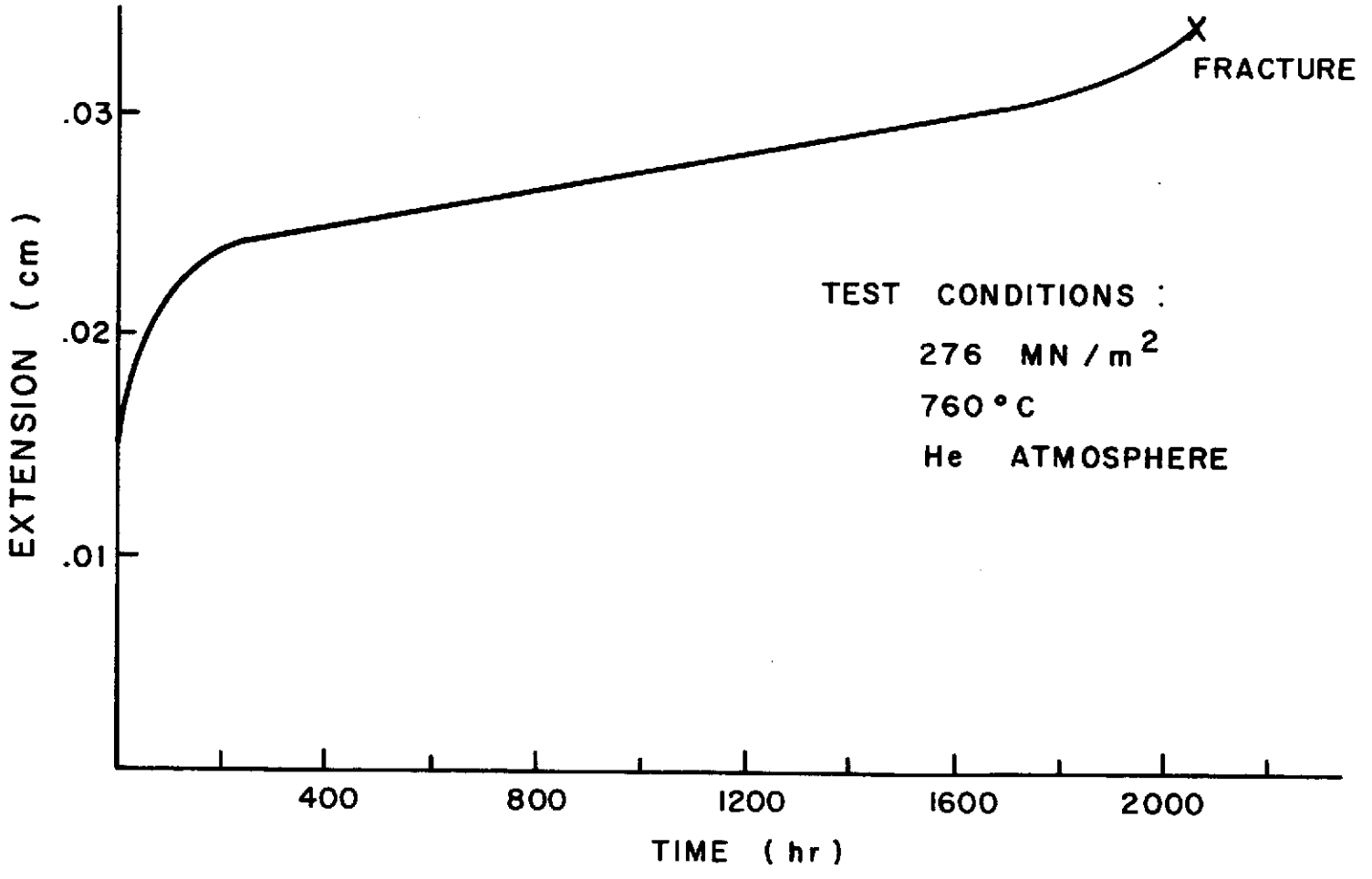

FIGURE 22: STRESS RUPTURE CURVE FOR Co-15 Cr-25 Ni - TaC DSE

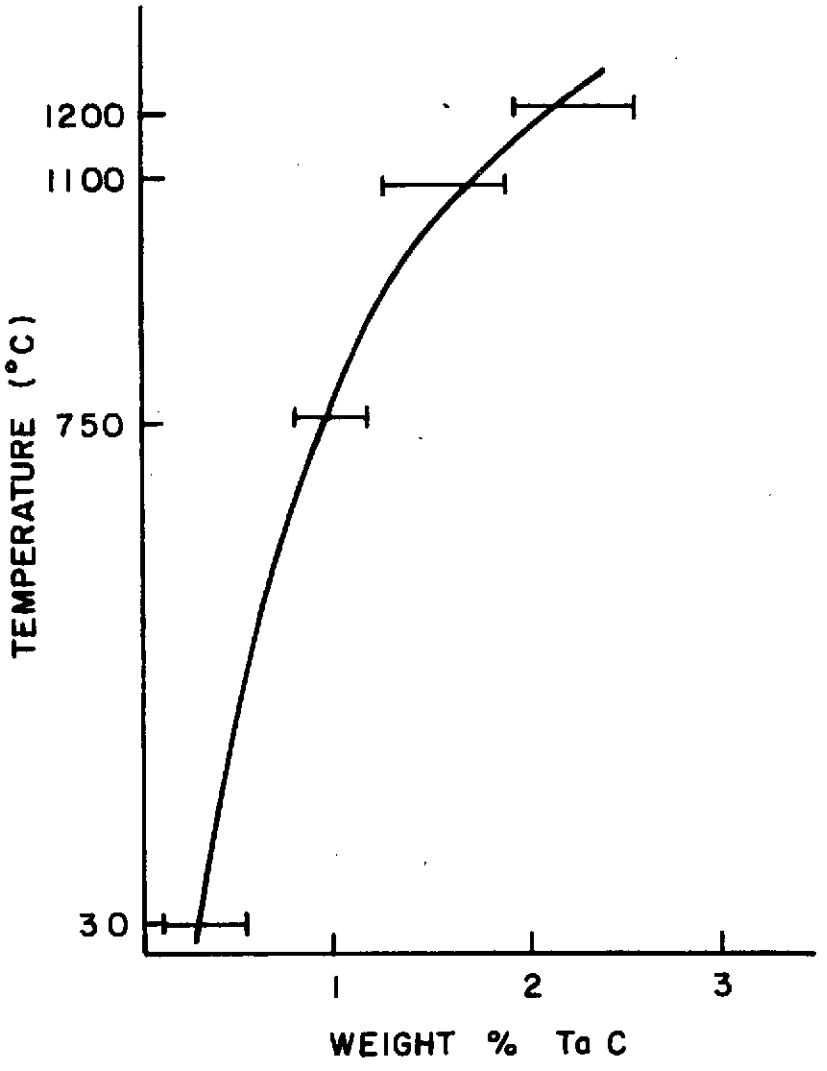

FIGURE 23 : SOLUBILITY OF TaC IN THE Co, Cr, Ni MATRIX

IX. APPENDIX A

The integrated intensities of the $(10.1)_{HCP}$ and $(200)_{FCC}$ reflections for the cobalt phases were obtained by diffractometer scans using electrolytically polished samples. The final polish was electrolytic to remove any transformation products which may have been produced during sample preparation. The data was converted to atomic % HCP using the following analysis.

Using the available data

$$a_{HCP} = 2.51 \text{ Å},$$
$$c_{HCP} = 4.07 \text{ Å},$$
$$a_{FCC} = 3.55 \text{ Å},$$

the atomic density for the diffracting planes are calculated:

0.26 atoms/Å^2 for HCP and
0.16 atoms/Å^2 for FCC[1].

The multiplicity for the HCP reflection is 12, and the mulplicity for the FCC reflection is 6 [2]. Using Co K_α radiation, the square of the scattering factor is 366 for HCP and 337 for the FCC.

Thus, the HCP phase is

$$(0.26 \times 12 \times 366)/(0.16 \times 6 \times 337) = 3.6$$

times as effective as the FCC phase in scattering x-rays for the reflections measured. The atomic % HCP is equal to

$$I_{HCP}/3.6 \times I_{FCC},$$

where I is the experimentally determined integrated intensity.

---

1. B. D. Cullity: Elements of X-Ray Diffraction, p. 462, Addison-Wesley, Reading, Mass., 1956.

2. L. V. Azaroff: Elements of X-Ray Crystallography, p. 201, McGraw Hill, New York, 1968.

3. International Tables for X-Ray Crystallography, vol. 3, Kynoch Press, Birmingham, England, 1968.

X. APPENDIX B

An estimate of the tensile strength of the TaC fibers is made using the rule of mixtures equation,

$$TS_c = TS_f(v) + TS_m(1-v),$$

where TS is the tensile strength and v is the volume fraction of the fibrous phase. The subscripts c, f, and m refer to the composite, fiber, and matrix.

The following were determined experimentally:

$$TS_c = 1035 \text{ MN/m}^2,$$
$$TS_m = 269 \text{ MN/m}^2,$$
$$v = 0.09.$$

Thus, TS_f is computed to be approximately 9000 MN/m^2.